

The Faintest Dwarf Galaxies

Joshua D. Simon¹

¹Observatories of the Carnegie Institution for Science, Pasadena, USA, 91101;
email: jsimon@carnegiescience.edu

Xxxx. Xxx. Xxx. Xxx. YYYY. AA:1–48

[https://doi.org/10.1146/\(please add article doi\)](https://doi.org/10.1146/(please add article doi))

Copyright © YYYY by Annual Reviews.
All rights reserved

Keywords

dark matter, dwarf galaxies, galaxy kinematics and dynamics, Local Group, metal-poor stars

Abstract

The lowest luminosity ($L < 10^5 L_{\odot}$) Milky Way satellite galaxies represent the extreme lower limit of the galaxy luminosity function. These ultra-faint dwarfs are the oldest, most dark matter-dominated, most metal-poor, and least chemically evolved stellar systems known. They therefore provide unique windows into the formation of the first galaxies and the behavior of dark matter on small scales. In this review, we summarize the discovery of ultra-faint dwarfs in the Sloan Digital Sky Survey in 2005, and the subsequent observational and theoretical progress in understanding their nature and origin. We describe their stellar kinematics, chemical abundance patterns, structural properties, stellar populations, orbits, and luminosity function, and what can be learned from each type of measurement. We conclude that: (1) In most cases, the stellar velocity dispersions of ultra-faint dwarfs are robust against systematic uncertainties such as binary stars and foreground contamination; (2) The chemical abundance patterns of stars in ultra-faint dwarfs require two sources of r-process elements, one of which can likely be attributed to neutron star mergers; (3) Even under conservative assumptions, only a small fraction of ultra-faint dwarfs may have suffered significant tidal stripping of their stellar components; (4) Determining the properties of the faintest dwarfs out to the virial radius of the Milky Way will require very large investments of observing time with future telescopes. Finally, we offer a look forward at the observations that will be possible with future facilities as the push toward a complete census of the Local Group dwarf galaxy population continues.

Contents

1. INTRODUCTION	2
1.1. The Cosmological Significance of the Lowest Luminosity Dwarf Galaxies	4
1.2. Defining “Ultra-Faint Dwarf”	5
2. STELLAR KINEMATICS	6
2.1. Mass Modeling and Dark Matter Content	8
2.2. Identification as Galaxies	14
3. METALLICITIES AND CHEMICAL ABUNDANCES	15
3.1. The Mass-Metallicity Relation	16
3.2. Metallicity Distribution Functions	18
3.3. Chemical Evolution Histories	18
3.4. Chemical Abundance Patterns	19
4. STRUCTURAL PROPERTIES	26
5. STELLAR POPULATIONS AND GAS CONTENT	26
5.1. Star Formation Histories	27
5.2. Initial Mass Functions	28
5.3. Gas Content	28
6. THE ULTRA-FAINT END OF THE GALAXY LUMINOSITY FUNCTION	29
7. ORIGIN AND EVOLUTION	30
7.1. The Formation of Ultra-Faint Dwarfs and the Stellar Mass-Halo Mass Relation	30
7.2. Galactic Orbits	32
7.3. Tidal Evolution	33
8. ULTRA-FAINT DWARFS AS DARK MATTER LABORATORIES	35
9. ULTRA-FAINT DWARFS BEYOND THE MILKY WAY	36
9.1. Ultra-Faint Dwarfs Around M31	36
9.2. Surveys Outside the Local Group	36
9.3. Connection to Observations of the High-Redshift Universe	37
10. SUMMARY AND OUTLOOK	38

1. INTRODUCTION

The search for faint dwarf galaxies has been a nearly continuous endeavor since the serendipitous discovery of the first such system, Sculptor, by Shapley (1938a). As significantly deeper survey data became available, systematic searches for more dwarfs slowly revealed what are now known as the classical dwarf spheroidal (dSph) satellites of the Milky Way (Shapley 1938b; Harrington & Wilson 1950; Wilson 1955; Cannon, Hawarden & Tritton 1977). However, after the identification of Sextans by Irwin et al. (1990), the push to ever lower luminosities and surface brightnesses stalled for more than a decade. New efforts to find faint, low surface brightness Milky Way dwarf galaxies continued fruitlessly in this period (Kleyna et al. 1997; Simon & Blitz 2002; Willman et al. 2002; Hopp, Schulte-Ladbeck & Kerp 2003; Whiting et al. 2007). Notably, though, there were strong theoretical reasons to expect that dwarfs with substantially lower luminosities and surface brightnesses should exist (Benson et al. 2002).

This prediction proved resoundingly correct in 2005, when the first such objects were discovered in Sloan Digital Sky Survey (SDSS) imaging by Willman et al. (2005a,b). These results opened the floodgates, and within two years the known population of Milky Way satellite galaxies more than doubled (Zucker et al. 2006b,a; Belokurov et al. 2006, 2007;

Sakamoto & Hasegawa 2006; Irwin et al. 2007; Walsh, Jerjen & Willman 2007). Over the following decade, new discoveries continued at a rapid pace in SDSS and other surveys (e.g., Belokurov et al. 2008, 2009, 2010; Bechtol et al. 2015; Koposov et al. 2015a, 2018; Drlica-Wagner et al. 2015, 2016; Martin et al. 2015; Kim et al. 2015a; Kim & Jerjen 2015; Laevens et al. 2015b,a; Torrealba et al. 2016b, 2018; Homma et al. 2016, 2018), such that the Milky Way satellite census has now doubled yet again (Figure 1). Thanks to significant investments of telescope time in deep imaging and spectroscopy of the newly discovered objects, along with accompanying theoretical modeling, we now have a general understanding of the properties of these systems and their place in galaxy evolution and cosmology.

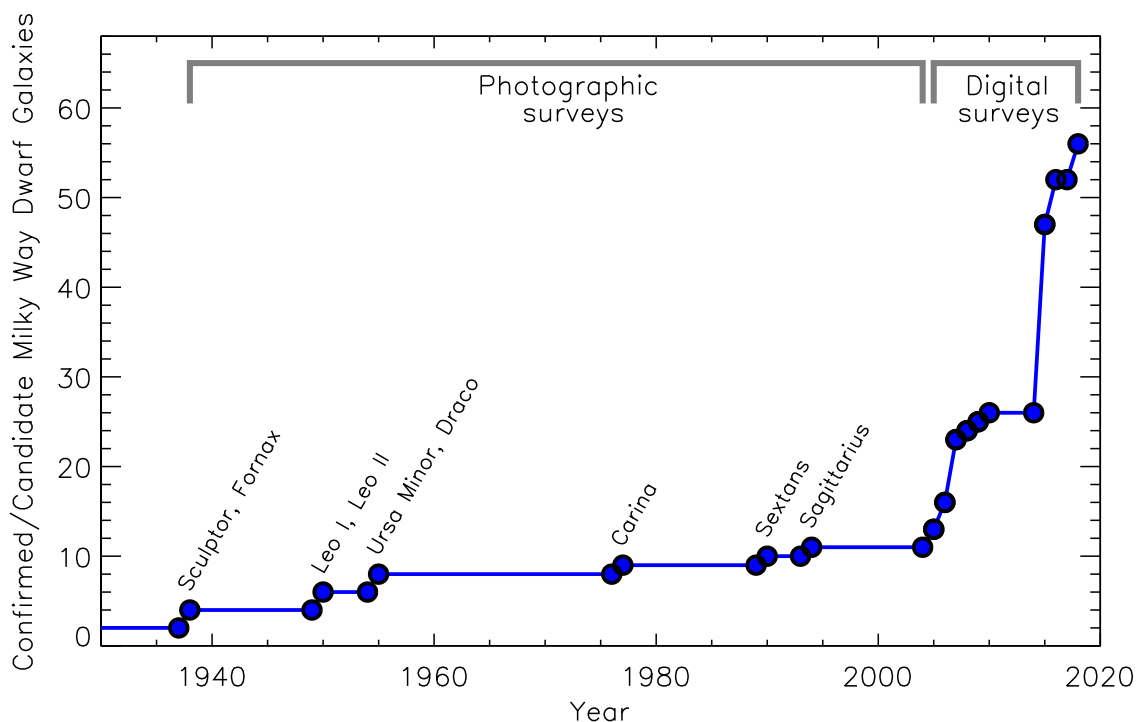


Figure 1 Census of Milky Way satellite galaxies as a function of time. The objects shown here include all spectroscopically confirmed dwarf galaxies as well as those suspected to be dwarfs based on less conclusive spectroscopic and photometric measurements. The major discovery impact of SDSS (from 2005-2010) and DES/Pan-STARRS (2015), each of which approximately doubled the previously known satellite population, stands out in this historical perspective.

While the faintest dwarf galaxies resemble globular clusters in some ways, when the population of low luminosity stellar systems is considered as a whole it is clear that they are galaxies rather than star clusters: (1) The stellar kinematics of ultra-faint dwarfs (UFDs) demonstrate that they contain significant amounts of dark matter; (2) All but the very

lowest-luminosity UFDs have physical extents larger than any known clusters; (3) Within each UFD, the abundances of Fe and α -elements exhibit substantial spreads resulting from extended star formation and internal chemical enrichment; (4) UFDs follow a luminosity-metallicity relationship, while globular clusters do not; (5) The abundances of certain elements in UFDs are similar to those in brighter dwarfs, and do not resemble the light element chemical abundance correlations seen in globular clusters. Each of these results is discussed in more detail in the remainder of this article.

In this review we summarize the progress that has been made in characterizing the least luminous galaxies since their discovery. We begin by motivating the study of the least luminous galaxies and by offering a definition of the term “ultra-faint dwarf,” which has been in common usage since the initial discoveries. In Section 2 we discuss the stellar kinematics and mass modeling of UFDs, and the corresponding evidence that they are galaxies rather than diffuse star clusters. In Section 3 we describe the metallicities and chemical abundance patterns of stars in UFDs, including the mass-metallicity relation, the chemical evolution of the smallest dwarfs, and their role in establishing the site of r-process nucleosynthesis. We briefly summarize the structural properties of the UFD population in Section 4. In Section 5 we introduce the star formation histories and initial mass functions of UFDs, and in Section 6 we examine constraints on the luminosity function of the faintest galaxies. We consider the origin and evolution of these systems based on theoretical work and measurements of their orbits around the Milky Way in Section 7. We provide a brief overview of the manifold ways in which UFDs may be used to constrain the behavior of dark matter in Section 8. In Section 9 we introduce the study of ultra-faint dwarfs outside the immediate neighborhood of the Milky Way and the connection between faint dwarfs in the Local Group and the high-redshift universe. In Section 10 we summarize the current state of the field and suggest future paths for research.

1.1. The Cosmological Significance of the Lowest Luminosity Dwarf Galaxies

A reasonable astronomer might ask how the smallest, most inconspicuous galaxies ever formed could have broad importance to the field of astrophysics. However, several aspects of the UFDs make them critical objects to understand, with potentially wide-ranging implications. First, UFDs reside in the smallest dark matter halos yet found. While only the mass at the very center of the halo is currently measurable, the extrapolated virial masses of UFDs are $\sim 10^9 M_\odot$ (e.g., Strigari et al. 2008), and the halo masses at the time when the stars formed may have been $\sim 10^8 M_\odot$ (e.g., Bovill & Ricotti 2009; Safarzadeh et al. 2018). UFDs are also the most dark matter-dominated systems known. This combination of small halo mass and negligible baryonic mass makes UFDs extremely valuable laboratories for constraining the nature of dark matter. Simply counting the number of such objects around the Milky Way places a limit on the mass of the dark matter particle (e.g., Jethwa, Erkal & Belokurov 2018). The census and observed mass function of low-mass halos will point the direction toward solving the long-standing and highly contentious missing satellite problem (e.g., Klypin et al. 1999; Moore et al. 1999; Simon & Geha 2007; Brooks et al. 2013; Kim, Peter & Hargis 2017). The measured central densities, and perhaps eventually the density profiles, of UFDs provide significant clues to the behavior of dark matter on small scales (e.g., Calabrese & Spergel 2016; Bozek et al. 2018; Errani, Peñarrubia & Walker 2018).

Second, UFDs represent the extreme limit of the galaxy formation process. They have

the lowest metallicities, oldest ages, smallest sizes, smallest stellar masses, and simplest assembly histories of all galaxies. Both observations and theoretical models indicate that UFDs formed at very high redshift, probably before the epoch of reionization. Unlike essentially all larger systems, they underwent little to no further evolution after that time, and have survived to the present day as pristine relics from the early universe (e.g., Bovill & Ricotti 2009, 2011; Wheeler et al. 2015). These objects therefore present us with a unique window into the conditions prevalent at the time when the first galaxies were forming.

To our knowledge, no previous reviews have focused primarily or exclusively on the properties of the faintest dwarf galaxies. Willman (2010) presented the first summary of searches for UFDs. There have been many reviews on the broader population of dwarfs (e.g., Mateo 1998; Tolstoy, Hill & Tosi 2009; McConnachie 2012, the latter two of which also discuss UFDs), and various aspects of UFDs have been featured in recent reviews on dark matter (e.g., Bullock & Boylan-Kolchin 2017; Strigari 2018) and metal-poor stars (e.g., Frebel & Norris 2015). Given the rapid maturation of the study of the very lowest luminosity galaxies over the last decade, here we aim to provide a comprehensive discussion of the current state of knowledge of these systems. After first results from LSST become available, some of this material may need to be revisited.

1.2. Defining “Ultra-Faint Dwarf”

The dwarf galaxies known prior to 2005 have absolute magnitudes brighter than $M_V = -8.7$, corresponding to V-band luminosities larger than $2.5 \times 10^5 L_\odot$. Their Plummer (half-light) radii are $\gtrsim 200$ pc, and with the exception of Sextans and Ursa Minor, their central surface brightnesses are < 26 mag arcsec $^{-2}$. In contrast, the dwarfs discovered in SDSS and other modern surveys are up to a factor of ~ 1000 less luminous, with half-light radii as small as ~ 20 pc and surface brightnesses that can be $\sim 2 - 3$ mag arcsec $^{-2}$ fainter than that of Sextans.

As was evident even from the titles of some of the first SDSS discovery papers — e.g., “A New Milky Way Companion: Unusual Globular Cluster or Extreme Dwarf Satellite?”¹ (Willman et al. 2005a) and “A Curious Milky Way Satellite in Ursa Major”² (Zucker et al. 2006a) — the nature of these new satellites was not immediately clear. Over the next several years, spectroscopy of stars in these objects pointed strongly to the conclusion that they were dwarf galaxies rather than globular clusters (Kleyna et al. 2005; Muñoz et al. 2006; Martin et al. 2007; Simon & Geha 2007). Given the clear differences in global properties relative to previously known dwarf galaxies, the community rapidly began referring to these objects as “ultra-faint” dwarfs, a term first used by Willman et al. (2005a). However, no formal definition of such a class was ever offered in the literature, and the usage of it has not been entirely consistent. In particular, Canes Venatici I (CVn I) is often referred to as a UFD because it was discovered in SDSS data around the same time as many fainter dwarfs (Zucker et al. 2006b), but its size and luminosity are nearly identical to those of Ursa Minor, which was identified more than 50 years earlier thanks to its location $\sim 3 \times$ closer to the Milky Way.

¹Indeed, the classification of Willman 1 is still not entirely secure, although the metallicities of its brightest member stars suggest that it is, or was, a dwarf galaxy (Willman et al. 2011).

²Although Zucker et al. (2006a) argued that Ursa Major II is a dwarf galaxy, the same system was identified independently by Grillmair (2006), who described it as “a new globular cluster or dwarf spheroidal.”

Despite this new nomenclature, it is now obvious that ultra-faint dwarfs continuously extend the properties of more luminous dwarfs in stellar mass, surface brightness, size, dynamical mass, and metallicity (see Figure 2 and Sections 2-4). They are not a physically distinct class of objects. Nevertheless, there are several reasons why it may be useful to refer to them via a separate label. In particular, UFDs represent the extreme end (we presume) of the distribution of galaxy properties, orders of magnitude beyond the previously-known dwarfs in some respects. Moreover, while classical dSphs can already be identified and studied in other nearby groups of galaxies, the UFDs are special in that only the very brightest examples of such systems will be detectable beyond the Local Group in the foreseeable future. Because of their lack of bright stars, detailed spectroscopic characterization of ultra-faint dwarfs will likely remain limited to satellites of the Milky Way. Finally, it is tempting to suggest that UFDs might differ from classical dSphs in that their star formation was shut off by reionization at $z \gtrsim 6$ instead of continuing to lower redshift. While this hypothesis is consistent with the available data, the sample of $M_V \gtrsim -9$ dwarf galaxies with precision star formation histories is too small to draw firm conclusions yet. If this idea turns out to be correct, it would provide a physically-motivated division between ultra-faint and classical dwarfs.

Based on the above discussion, we suggest that dwarf galaxies with absolute magnitudes fainter than $M_V = -7.7$ ($L = 10^5 L_\odot$) be considered UFDs. This definition matches the naming convention adopted by Bullock & Boylan-Kolchin (2017). Among the post-2005 discoveries, only four galaxies are within 1 magnitude of this boundary: CVn I ($M_V = -8.7$), Crater II ($M_V = -8.2$), Leo T ($M_V = -8.0$), and Eridanus II ($M_V = -7.2$). The first three of these systems stand out from the fainter population in obvious ways: CVn I is substantially more luminous, larger, and more metal-rich (e.g., Martin et al. 2007; Martin, de Jong & Rix 2008; Simon & Geha 2007; Muñoz et al. 2018), Crater II is a factor of ~ 4 more extended than any fainter dwarf (Torrealba et al. 2016a), and Leo T hosts neutral gas and recent star formation (Ryan-Weber et al. 2008; de Jong et al. 2008). These objects more closely resemble the previously-known dSphs and dSph/dIrrs in the Local Group. Eridanus II, on the other hand, is distinct from other UFDs only in that it contains a star cluster (Crnojević et al. 2016b). Setting the dividing line such that it lands between Eridanus II and Leo T is therefore sensible, and minimizes the likelihood that future revisions to the absolute magnitudes of any of these systems will blur the boundary.

2. STELLAR KINEMATICS

Following their discovery, the first important step in clarifying the nature of the UFDs was to determine their stellar velocity dispersions. By measuring the velocities of individual stars in several systems, these early studies constrained their dynamical masses and dark matter content.

The initial spectroscopic observations of UFDs were made by Kleyna et al. (2005) for Ursa Major I (UMa I) and Muñoz et al. (2006) for Boötes I (Boo I). Using Keck/HIRES spectra of 5 stars, Kleyna et al. measured a velocity dispersion of $\sigma = 9.3_{-1.2}^{+11.7}$ km s⁻¹. Muñoz et al. determined a velocity dispersion of $\sigma = 6.6 \pm 2.3$ km s⁻¹ from WIYN/Hydra spectra of 7 Boo I stars. These two systems have luminosities of 9600 and 21900 L_\odot , respectively. If the stellar mass-to-light ratio is $\approx 2 M_\odot/L_\odot$ (as expected for an old stellar population with a standard initial mass function), then the expected velocity dispersions from the stellar mass alone would be $\lesssim 0.1$ km s⁻¹ (making use of the Wolf et al. 2010 mass

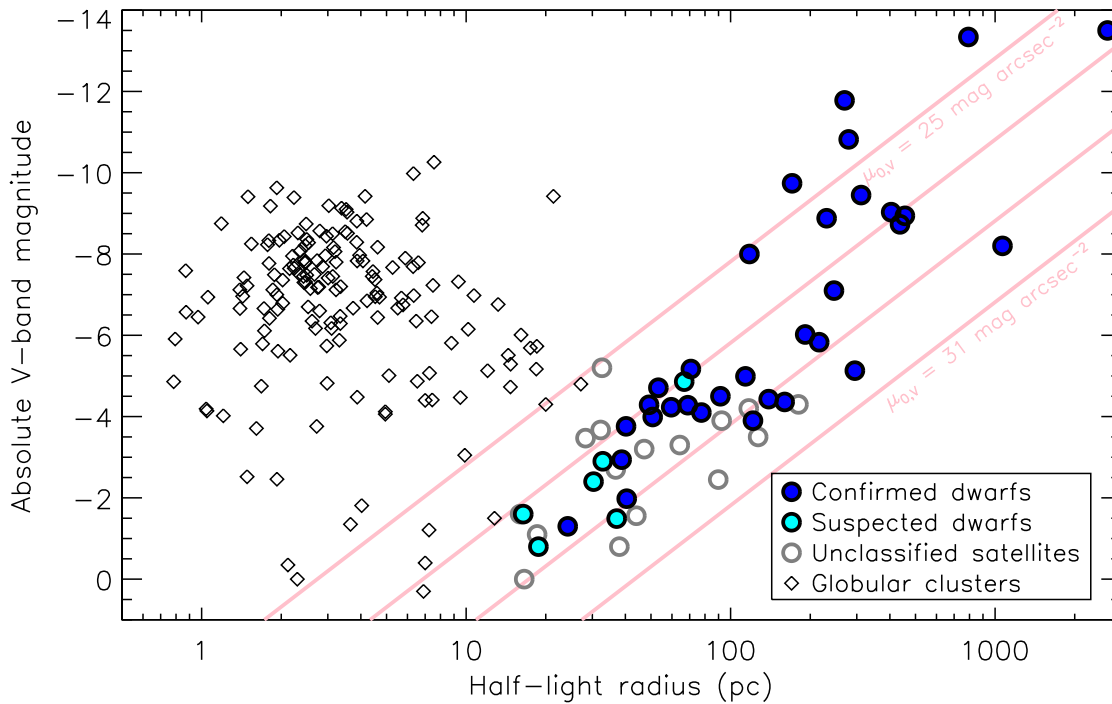


Figure 2 Distribution of Milky Way satellites in absolute magnitude (M_V) and half-light radius. Confirmed dwarf galaxies are displayed as dark blue filled circles, and objects suspected to be dwarf galaxies but for which the available data are not conclusive are shown as cyan filled circles. Dwarf galaxy candidates without any published classification (usually because of the lack of spectroscopy) are shown as open gray circles. The faint candidates with $R_{1/2} \gtrsim 50$ pc are almost certainly dwarf galaxies, but we do not include them in the confirmed category here given the currently available observations. The dwarf galaxy/candidate data included in this plot are listed in Table 1. The black diamonds represent the Milky Way’s globular clusters (Harris 1996). Lines of constant central surface brightness (at 25, 27, 29, and 31 mag arcsec^{-2} in V band) are plotted in pink. For stellar systems brighter than $M_V \approx -5$ there is no ambiguity in classification: globular clusters have $R_{1/2} \lesssim 20$ pc and dwarf galaxies have $R_{1/2} \gtrsim 100$ pc. At fainter magnitudes the size distributions begin to impinge upon each other and classification based purely on photometric parameters may not always be possible. Whether the two populations actually occupy non-overlapping portions of this parameter space remains to be determined from spectroscopy of the faintest stellar systems with half-light radii between 10 and 40 pc.

estimator). In both cases, such a small velocity dispersion can be ruled out at high significance, demonstrating that under standard assumptions UFDs cannot be purely baryonic systems. Similar conclusions quickly followed for the remaining ultra-faint dwarfs based on

analyses of Keck/DEIMOS spectroscopy by Martin et al. (2007) and Simon & Geha (2007). At the present, velocity dispersion measurements or limits have been obtained for 27 out of 42 confirmed or candidate UFDs. All of the available kinematic data are displayed in Figure 3.

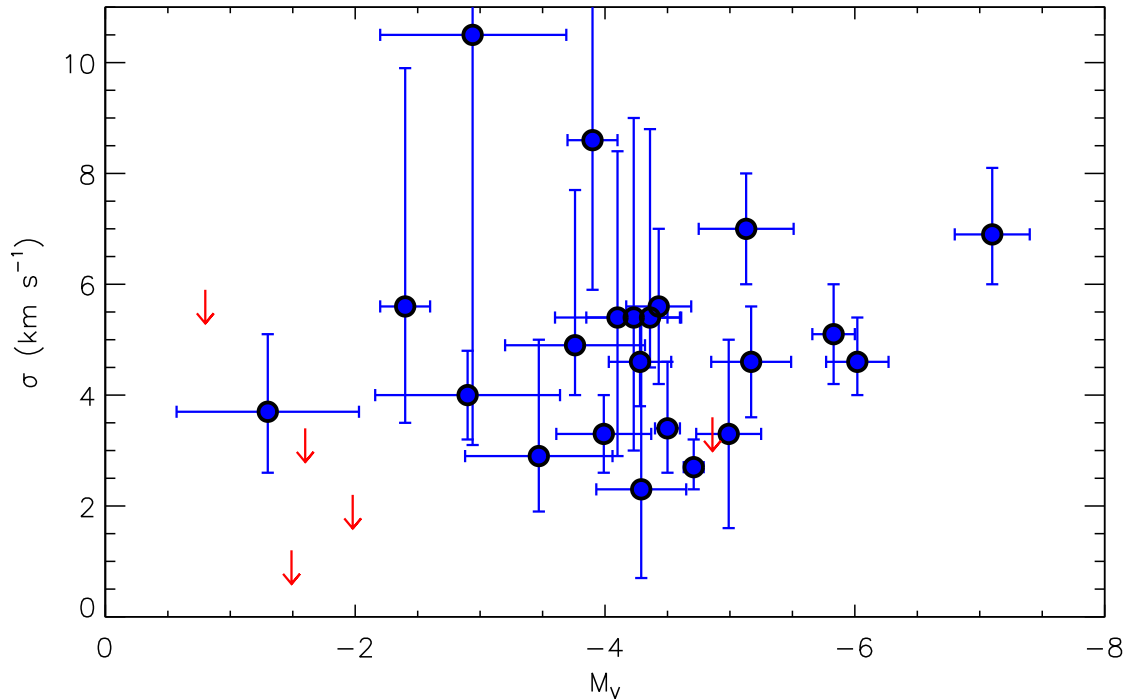


Figure 3 Line-of-sight velocity dispersions of ultra-faint Milky Way satellites as a function of absolute magnitude. Measurements and uncertainties are shown as the blue points with error bars, and 90% confidence upper limits are displayed as red arrows for systems without resolved velocity dispersions. The dwarf galaxy data included in this plot are listed in Table 1. Although there is a clear trend of decreasing velocity dispersion toward fainter dwarfs among the classical dSphs, in the ultra-faint luminosity regime there is much more scatter and any systematic trend is weak.

2.1. Mass Modeling and Dark Matter Content

2.1.1. Assumptions Required for Determining Masses. The results shown in Figure 3 are simply measurements: the observed dispersion of the radial velocities for the set of stars in each dwarf for which spectra were obtained. In order to translate these velocity dispersions into dynamical masses, several assumptions must be made. First, no inference can be drawn about the mass of a system unless it is in dynamical equilibrium. If a dwarf galaxy has experienced, for example, a recent tidal shock, then its present velocity dispersion may not

be a reliable indicator of its mass. Recent proper motion measurements show that many of the ultra-faint dwarfs are indeed close to their orbital pericenters, but those pericentric passages occur at typical distances of nearly 40 kpc away from the Galactic center, lessening their impact (Simon 2018). While the assumption of equilibrium deserves further attention in modern high-resolution simulations, earlier studies indicate that even when dwarf galaxies have been tidally disturbed their velocity dispersions do not change substantially, and the instantaneous dispersion remains a good barometer of the bound mass (Oh, Lin & Aarseth 1995; Piatek & Pryor 1995; Muñoz, Majewski & Johnston 2008).

Second, unless spectroscopy of a dwarf is obtained over multiple, well-separated observing runs, it must be assumed that binary stars are not inflating the observed velocity dispersion above its true value. The influence of binary stars may be particularly concerning given the recent suggestion that the binary fraction is quite large at low metallicities (Moe, Kratter & Badenes 2018). Several individual binary stars have been detected in UFDs (e.g., Frebel et al. 2010; Koposov et al. 2011; Koch et al. 2014; Ji et al. 2016c; Kirby et al. 2017; Li et al. 2018b), and the binary population of Segue 1 was evaluated statistically by Martinez et al. (2011) and Simon et al. (2011). Only the binary system in Hercules identified by Koch et al. (2014) has an orbit solution (with period 135.28 ± 0.33 d and velocity semi-amplitude 14.48 ± 0.82 km s⁻¹), but the few other UFD binaries with detected velocity variability appear to have semi-amplitudes of $\sim 10 - 20$ km s⁻¹ and periods $\lesssim 1$ yr as well (Ji et al. 2016c; Kirby et al. 2017; Li et al. 2018b). Frebel, Simon & Kirby (2014) also found indirect evidence of binarity for a star in Segue 1 based on its chemical abundances, which are best explained by mass transfer from a (formerly) more massive companion star.

In the classical dSphs, a number of studies have shown that binary stars do not significantly inflate the observed velocity dispersions (e.g., Olszewski, Aaronson & Hill 1995; Olszewski, Pryor & Armandroff 1996; Vogt et al. 1995; Hargreaves, Gilmore & Annan 1996; Kleyna et al. 2002; Minor et al. 2010; Spencer et al. 2017). It has also been suggested, however, that the effect of binaries may be larger in UFDs given their smaller intrinsic velocity dispersions (McConnachie & Côté 2010; Spencer et al. 2017). While that is certainly true in principle, observationally most UFD data sets do not seem to be significantly affected by binaries. For example, removing the radial velocity variables from the sample of Boo I stars analyzed by Koposov et al. (2011) changes the velocity dispersion by only $\sim 3\%$.³ Similarly, Martinez et al. (2011) and Simon et al. (2011) corrected the effects of binaries in Segue 1 with Bayesian modeling of a multi-epoch radial velocity data set and found that the binary-corrected velocity dispersion agrees within the uncertainties with the uncorrected dispersion. Other recent studies have also included multi-epoch velocity measurements, either finding no obvious binaries (Simon et al. 2017) or removing the binaries before computing velocity dispersions (Li et al. 2018b). On the other hand, there are at least two examples of binary stars indeed biasing the derived velocity dispersions of UFDs: Ji et al. (2016c), Venn et al. (2017), and Kirby et al. (2017) showed that Boötes II (Boo II) and Triangulum II (Tri II) each contain a bright star in a binary system that was responsible for substantially increasing the velocity dispersions determined by Koch et al. (2009) for Boo II and by Martin et al. (2016b) and Kirby et al. (2015) for Tri II. In both of

³Here we are modeling the Boo I velocity distribution as a single Gaussian for simplicity. Koposov et al. (2011) argued that the data are better described by a two-component model, with a majority of the stars in a cold $\sigma = 2.4_{-0.5}^{+0.9}$ km s⁻¹ component and $\sim 30\%$ in a hotter component with $\sigma \approx 9$ km s⁻¹, but they were not able to rule out a single-Gaussian model.

these cases, the influence of the binary was magnified by the very small samples of radial velocities available (5 stars in Boo II and 6 – 13 stars in Tri II). These results indicate that while binary stars do not significantly change the velocity dispersions of most ultra-faint dwarfs, studies consisting of single-epoch velocity measurements of small numbers of stars should be interpreted with caution.

Finally, an often unstated assumption is that samples of ultra-faint dwarf member stars are free from contamination by foreground Milky Way stars. Contamination is a particularly tricky issue for galaxies with velocities close to the median velocity of Milky Way stars along that line of sight (e.g., Willman 1, Hercules, and Segue 2⁴), although incorrectly identified members are possible in any dwarf. Because stars that could be mistaken for UFD members must have velocities close to the systemic velocity of the dwarf, the effect of such contaminants is likely more severe for the derived metallicity distribution than the velocity dispersion (e.g., Siegel, Shetrone & Irwin 2008; Kirby et al. 2017). Several examples of erroneously determined UFD members are available in the literature. Simon (2018) demonstrated that stars previously classified as members of Ursa Major I (UMa I) by Kleyna et al. (2005) and Simon & Geha (2007) and Hydrus I (Hyi I) by Koposov et al. (2018) have *Gaia* proper motions that strongly disagree with the remaining members. Removing these stars from the member samples reduces the UMa I velocity dispersion from $7.6 \pm 1.0 \text{ km s}^{-1}$ to $7.0 \pm 1.0 \text{ km s}^{-1}$ and has no effect on the measured dispersion of Hyi I. Similarly, Frebel et al. (2010) obtained a high-resolution spectrum of a star identified by Simon & Geha (2007) as an Ursa Major II (UMa II) member but found that its surface gravity was not consistent with that classification; the velocity dispersion of UMa II is not significantly changed by the exclusion of this star. Adén et al. (2009) argued using Strömrgren photometry that the Hercules member sample from Simon & Geha (2007) was contaminated by several non-member stars, but the derived velocity dispersions are only 1.1σ apart.

For the classical dSphs, where large member samples of hundreds to thousands of stars are generally available, a common method for dealing with foreground contamination is to make use of membership probabilities for each star (e.g., Walker et al. 2009b; Caldwell et al. 2017). These probabilities are determined via a multi-component model of the entire data set, e.g., assuming Gaussian velocity and metallicity distributions and a Plummer (1911) radial profile for the dwarf galaxy. The global properties of the dwarf can then be computed using the individual membership probabilities as weights, with a star with a membership probability of 0.5 counting half as much as a certain member with a probability of 1.0. In the limit where there are many stars with intermediate membership probabilities ($0.1 \lesssim p_{\text{mem}} \lesssim 0.9$), some of which are genuine members and some of which are foreground stars, the

⁴We take this opportunity to note that the standard nomenclature for new stellar systems discovered in the Local Group for the past several decades has been that dwarf galaxies are named after the constellations in which they are located, while globular clusters are named after the survey in which they were found or the author who identified them. When multiple discoveries are made in a single constellation or survey, dwarfs are usually numbered with Roman numerals and globular clusters with Arabic numbers. One drawback of this convention is that it is no longer always obvious when an object is discovered how to classify it. Consequently, Willman 1 and Segue 1 and 2 were named as if they were globular clusters and then later realized to be dwarf galaxies. The community now appears to be hopelessly confused about whether their numbering should be Roman or Arabic (the answer is Arabic; once a name is established it is not worth changing). The question going forward is whether past naming conventions should be continued, if new conventions should be adopted, or if temporary names should be used until a robust classification is available.

reduced contributions of actual members and the increased contributions of contaminants can reasonably be assumed to cancel out so that the derived properties of the system are accurate. It is less clear, however, that this statistical approach works well when applied to the small data sets typical for UFDs. For example, the stars with ambiguous membership status are likely to be those that are outliers from the remainder of the population in velocity and/or metallicity. In reality, of course, each such star is either a member of the dwarf or not. If there is only a single star in this category, probabilistically including it as, say, 0.5 member stars may substantially change the inference on the velocity or metallicity dispersion of the system. In the shot noise-limited regime, a better approach to deal with outliers may be simply to report the derived values with and without the questionable star(s) included, acknowledging the resulting uncertainty. Fortunately, the advent of *Gaia* astrometry should make it possible to correctly classify most stars whose membership would previously have been uncertain, reducing the importance of this issue going forward.

2.1.2. Dynamical Masses and Dark Matter. Once the assumptions of dynamical equilibrium and minimal contamination by binary stars and foreground stars are made, the observed velocity dispersion can be used to constrain the mass of a dwarf galaxy. Early work (e.g., Kleyana et al. 2005; Muñoz et al. 2006; Martin et al. 2007; Simon & Geha 2007) relied on the method of Illingworth (1976) for determining globular cluster masses, as applied by Mateo (1998) to dSphs. The Illingworth formula is based on the dynamical model developed by King (1966), again for globular clusters. As discussed by Wolf et al. (2010), several key assumptions of this method fail (or may fail) in the case of dwarf galaxies. In order of increasing severity, these assumptions include that (1) the velocity dispersion is independent of radius, (2) the velocity dispersion is isotropic, and (3) the mass profile follows the light profile. An alternate formalism is therefore needed; in particular, one in which the mass is not assumed to be distributed in the same way as the light.

Wolf et al. (2010) showed that for dispersion-supported stellar systems with unknown velocity anisotropy, the mass that is most tightly constrained by stellar velocity measurements is the mass enclosed within the three-dimensional half-light radius of the system, $M_{1/2} = M(< r_{1/2,3D})$. This approach still requires that the velocity dispersion profile be approximately flat in the measured region (which is generally the case in the dwarf galaxies for which that measurement can be made), but does not assume anything about the shape of the anisotropy profile or the mass distribution. According to Wolf et al. (2010),

$$M_{1/2} = 930 \left(\frac{\sigma}{\text{km s}^{-1}} \right)^2 \left(\frac{R_{1/2}}{\text{pc}} \right) M_{\odot}, \quad 1.$$

where σ is the velocity dispersion and $R_{1/2}$ is the projected two-dimensional half-light radius.⁵ (One can also write this relation in terms of the deprojected three-dimensional half-light radius, $r_{1/2}$, but that is less convenient since $R_{1/2}$ is what can be measured directly. For many light profiles the two are simply related by $r_{1/2} = \frac{4}{3}R_{1/2}$, as shown by Wolf et al. 2010.)

The dynamical masses determined with Equation 1 are displayed in Figure 4. Every UFD for which the velocity dispersion has been measured has a mass of at least $10^5 M_{\odot}$ within its half-light radius. Among the five systems with only upper limits on the dispersion

⁵Similar relations have been derived by Walker et al. (2009a) and Errani, Peñarrubia & Walker (2018).

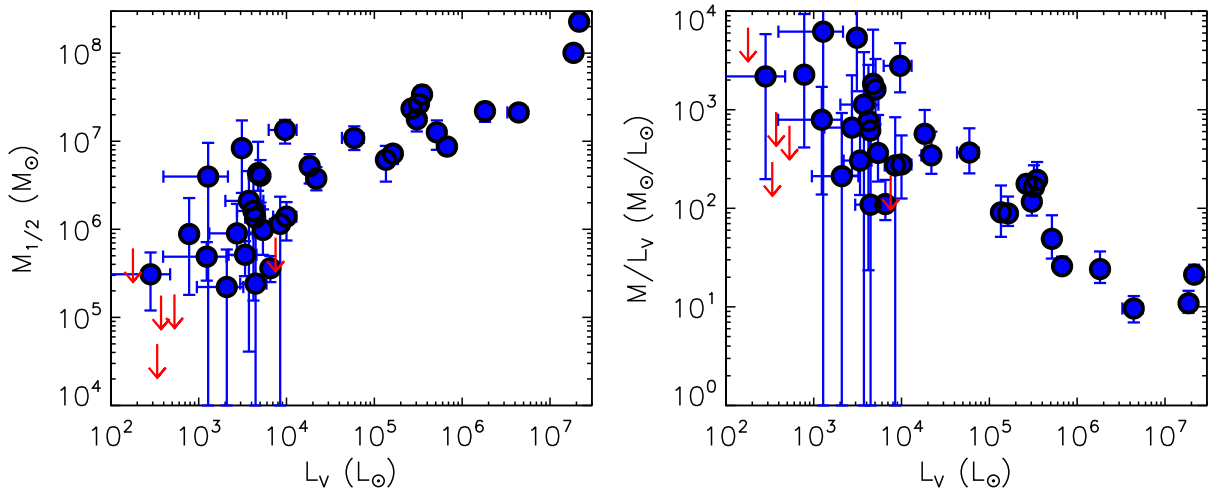


Figure 4 (*left*) Dynamical masses of ultra-faint Milky Way satellites as a function of luminosity. (*right*) Mass-to-light ratios within the half-light radius for ultra-faint Milky Way satellites as a function of luminosity. Measurements and uncertainties are shown as the blue points with error bars, and mass limits determined from the 90% confidence upper limits on the dispersion are displayed as red arrows for systems without resolved velocity dispersions. The dwarf galaxy/candidate data included in this plot are listed in Table 1.

available, all but Tucana III (Tuc III) are consistent with such masses as well. In comparison, the luminosities are a factor of ~ 100 or more smaller. Given that the stellar mass-to-light ratio is $\sim 2 M_{\odot}/L_{\odot}$ for an old stellar population with a Salpeter (1955) initial mass function⁶ (e.g., Martin, de Jong & Rix 2008), it is clear that nearly all of the UFDs have masses that are dominated by something other than their stars.

2.1.3. Galaxies for which Published Kinematics May Not Reliably Translate to Masses.

The reported stellar kinematics and corresponding masses of UFDs often seem to be regarded as having uniform reliability, especially by those other than the original observers. In fact, however, there are wide variations from galaxy to galaxy in how well determined the internal kinematics are. The size of the member sample, the quality of the individual velocity measurements, and the evolutionary history of the object in question all influence the degree to which accurate dynamical inferences can be made. Some specific objects that should be treated with caution include:

- *Willman 1* — Although Willman et al. (2011) identified a sizable sample of 40 likely Willman 1 member stars with high-quality Keck/DEIMOS velocity measurements, the internal kinematics of Willman 1 defy straightforward interpretation. The stars closest to the center of Willman 1 differ in velocity by 8 km s^{-1} from the remainder of the system, and their velocity dispersion is consistent with zero. While it is possible

⁶A Kroupa (2001) or other shallower IMF (e.g., Geha et al. 2013) has an even smaller stellar mass-to-light ratio.

that this configuration is simply the result of small number statistics, it could also indicate that the assumption of dynamical equilibrium is not valid for Willman 1. On the other hand, as already pointed out by Willman et al. (2011), tidal forces would not obviously cause such a velocity distribution.

- *Boo II* — Koch et al. (2009) measured a velocity dispersion of $10.4 \pm 7.5 \text{ km s}^{-1}$ for Boo II using Gemini/GMOS spectra of 5 member stars. The small sample of members and the presence of at least one binary star, as mentioned above, combine to compromise this measurement (Ji et al. 2016c). A dedicated study of a larger set of Boo II stars will likely show that the velocity dispersion of Boo II is substantially smaller, in line with those of the other UFDs.
- *UMa II* — UMa II has been the subject of two kinematic studies: Martin et al. (2007) determined a velocity dispersion of $7.4^{+4.5}_{-2.8} \text{ km s}^{-1}$ from Keck/DEIMOS spectroscopy of 11 members, and Simon & Geha (2007) measured a dispersion of $6.7 \pm 1.4 \text{ km s}^{-1}$, also with Keck/DEIMOS, for a sample of 20 members. The large velocity dispersion of UMa II, combined with its relatively close distance, have been used to argue that it is one of the most promising targets for the indirect detection of dark matter (e.g., Ahnen et al. 2018). One of the Simon & Geha members is now known to be a foreground contaminant (see above), but this star does not impact the velocity dispersion. Subsequent to the velocity dispersion measurements, one binary star was detected in UMa II by Frebel et al. (2010). Removing these two stars from the sample reduces the velocity dispersion to $5.6 \pm 1.4 \text{ km s}^{-1}$, but we also note that most of the other UMa II members have not been checked for binarity. Furthermore, UMa II is the only UFD for which the typical Plummer or exponential radial profiles fail to provide a good fit (Muñoz, Geha & Willman 2010; Muñoz et al. 2018). Its unusual profile may be consistent with tidal disruption (Muñoz, Geha & Willman 2010), but on the other hand, the orbit of UMa II has a pericenter of 39^{+2}_{-3} kpc and a long period of $\sim 3.5 \text{ Gyr}$, suggesting that the dwarf has completed at most 3 orbits around the Milky Way and has never approached closely enough for its stars to be tidally stripped (Simon 2018). Verifying that UMa II indeed has a larger velocity dispersion than other UFDs and is in equilibrium will require spectroscopy of a larger sample of stars over a wider area, as well as repeat velocity measurements to check for the binarity of known members.
- *Boo I* — Koposov et al. (2011) presented a high-quality VLT/FLAMES kinematic data set for Boo I. They showed that, unlike other UFDs, its line of sight velocity distribution is best described by two distinct components, one with a dispersion of $2.4^{+0.9}_{-0.5} \text{ km s}^{-1}$ and the other with a dispersion of $\approx 9 \text{ km s}^{-1}$. These components are reminiscent of the multiple populations with separate radial, metallicity, and velocity distributions seen in some of the more luminous dSphs (e.g., Tolstoy et al. 2004; Battaglia et al. 2006, 2011). However, in Boo I the available stellar samples are too small to confidently detect the photometric or chemical signatures of two populations (Koposov et al. 2011). In the absence of a half-light radius to associate with each kinematic component, we emphasize that using one of the cold or hot velocity dispersions alone to calculate the mass of Boo I is not valid.

2.2. Identification as Galaxies

Prior to the discovery of dwarf galaxies fainter than $M_V \sim -5$, dwarfs and globular clusters occupied distinct and cleanly separated portions of the size-luminosity parameter space displayed in Fig. 2. Consequently, there was little discussion of whether certain objects should be considered to be galaxies or clusters; the classification of all known systems was obvious.⁷

As the dwarf galaxy population grew toward lower luminosities and smaller radii, the gap between dwarfs and globular clusters in the size-luminosity plane disappeared, such that size alone was no longer sufficient to determine the nature of an object. Conn et al. (2018) dubbed the region occupied by a number of ultra-faint satellites ($14 < r_{1/2} < 25$ pc) the “trough of uncertainty” to emphasize the difficulty in classifying these systems. In order to resolve the confusion caused by the lack of an agreed-upon system for separating galaxies from star clusters, Willman & Strader (2012) proposed the following definition:

“A galaxy is a gravitationally bound collection of stars whose properties cannot be explained by a combination of baryons and Newton’s laws of gravity.”

Applied to UFDs, this definition is generally interpreted as requiring an object to have either a dynamical mass significantly larger than its baryonic mass or a non-zero spread in stellar metallicities to qualify as a galaxy. The former criterion directly indicates the presence of dark matter (for which there is no evidence in globular clusters), while the latter indirectly suggests that the object must be embedded in a dark matter halo massive enough that supernova ejecta can be retained for subsequent generations of star formation.

The early SDSS UFDs were all measured to have velocity dispersions larger than 3 km s^{-1} , implying that they are composed mostly of dark matter and can be straightforwardly classified as galaxies (Kleyna et al. 2005; Muñoz et al. 2006; Martin et al. 2007; Simon & Geha 2007; Geha et al. 2009). Some disagreement persisted for several years regarding the nature of the two least-luminous systems, Willman 1 and Segue 1 (e.g., Belokurov et al. 2007; Siegel, Shetrone & Irwin 2008; Niederste-Ostholt et al. 2009), but ultimately the combination of stellar kinematics, metallicities, and chemical abundance measurements led to the conclusion that both are dwarfs (Willman et al. 2011; Simon et al. 2011; Frebel, Simon & Kirby 2014). The first object for which kinematic classification failed entirely was Segue 2. Despite a comprehensive analysis of the kinematics of Segue 2, Kirby et al. (2013a) were unable to measure its velocity dispersion, finding $\sigma < 2.6 \text{ km s}^{-1}$ at 95% confidence. With only an upper limit on the dynamical mass and mass-to-light ratio, it cannot be confirmed that Segue 2 contains dark matter. However, Kirby et al. also showed that the stars of Segue 2 span a large range of metallicities, from $[\text{Fe}/\text{H}] = -2.9$ to $[\text{Fe}/\text{H}] = -1.3$, with a dispersion of 0.43 dex. Segue 2 can therefore still be classified as a galaxy rather than a globular cluster on the basis of its chemical enrichment.

The discovery of larger numbers of compact ultra-faint satellites in Dark Energy Survey and Pan-STARRS data (Bechtol et al. 2015; Koposov et al. 2015a; Drlica-Wagner et al. 2015; Laevens et al. 2015b,a) has increased the difficulty in classification. For several of these objects only upper limits on the velocity dispersion have been obtained (Kirby, Simon

⁷The exception to this statement is the idea that some globular clusters, most notably ω Centauri, might be the remnant nuclei of tidally disrupted dwarf galaxies (e.g., Lee et al. 1999; Majewski et al. 2000; Hilker & Richtler 2000).

& Cohen 2015; Kirby et al. 2017; Martin et al. 2016a; Simon et al. 2017), and in the case of Tuc III no metallicity dispersion is detectable in current data either (Simon et al. 2017). In such situations one must either accept the uncertainty in the nature of some systems or rely on more circumstantial arguments such as size, survival in a strong tidal field (e.g., Simon et al. 2017), mass segregation (Kim et al. 2015b), or chemical peculiarities.

As of this writing, the following 21 satellites can be regarded as spectroscopically confirmed ultra-faint dwarf galaxies: Segue 2, Hydrus 1, Horologium I, Reticulum II, Eridanus II, Carina II, Ursa Major II, Segue 1, Ursa Major I, Willman 1, Leo V, Leo IV, Coma Berenices, Canes Venatici II, Boötes II, Boötes I, Hercules, Pegasus III, Aquarius II, Tucana II, and Pisces II. Satellites that may be dwarfs but for which either no spectroscopy has been published or the data are inconclusive include: Tucana IV, Cetus II, Cetus III, Triangulum II, DES J0225+0304, Horologium II, Reticulum III, Pictor I, Columba I, Pictor II, Carina III, Virgo I, Hydra II, Draco II, Sagittarius II, Indus II, Grus II, Grus I, Tucana V, Phoenix II, and Tucana III. The most extended of these objects, such as Tucana IV, Cetus III, Columba I, and Grus II, are perhaps the most likely to be dwarfs given their large radii. We have not included Boötes III, which is likely the remnant of a dwarf, in either category because it is not clear whether it is still a bound object (Grillmair 2009; Carlin et al. 2009; Carlin & Sand 2018).

The problem of determining the nature of the faintest and most compact Milky Way satellites will only become more severe in coming years as surveys become sensitive to even lower luminosity, lower surface brightness, and more distant stellar systems. Spectroscopic follow-up of the satellites discovered by LSST will require massive investments of telescope time on either existing facilities or those currently under consideration (Najita et al. 2016).

3. METALLICITIES AND CHEMICAL ABUNDANCES

The metallicities of stars in UFDs are important both for classifying them as galaxies (Section 2.2) and for connecting them to the broader field of galaxy formation (Section 9.3). Fortunately, the same spectra of individual stars from which the stellar kinematics are determined can often be used to measure metallicities. With spectral synthesis techniques developed over the last decade and other methods, abundances of several elements other than iron can also be obtained from medium-resolution spectra of dwarf galaxy stars (e.g., Kirby et al. 2009; Norris et al. 2010b; Kirby et al. 2011; Vargas et al. 2013; Koposov et al. 2015b). Mean metallicities based on such data have now been obtained for 26 out of 42 confirmed/candidate UFDs. Detailed chemical abundance patterns generally require observations at higher spectral resolution, which are challenging for dwarf galaxies because even their brightest stars are usually rather faint.

The first spectroscopic metallicity measurements for ultra-faint dwarfs were provided by Muñoz et al. (2006), Martin et al. (2007), and Simon & Geha (2007). Collectively, these studies showed that the ultra-faint dwarfs have very low metallicities ($[\text{Fe}/\text{H}] \lesssim -2$) and that the stars in each object span a range in metallicity. The latter property distinguishes UFDs from globular clusters, and indicates both that star formation in these objects extended for a long enough period of time for supernova (SN) enrichment to occur and that their gravitational potential is deep enough that not all of the supernova ejecta can escape the system. Kirby et al. (2008) used more accurate metallicity measurements to show that many of the ultra-faint dwarfs contain extremely metal-poor (EMP) stars with $[\text{Fe}/\text{H}] < -3$, again distinct from globular clusters and (at the time) classical dSphs.

UFDs are particularly appealing systems in which to study early chemical evolution and nucleosynthesis because their small stellar masses imply that they have hosted relatively few SN explosions. That fact, combined with the short time periods during which they were forming stars (see Section 5), means that UFDs may preserve the unpolluted chemical signatures of small numbers of nucleosynthetic events (Bland-Hawthorn et al. 2010; Karlsson, Bromm & Bland-Hawthorn 2013), perhaps even individual explosions (e.g., Frebel & Bromm 2012; Ji, Frebel & Bromm 2015). Koch et al. (2008) began the process of analyzing the detailed chemical abundances of UFD stars with high-resolution Magellan/MIKE spectra of two stars in Hercules. Frebel et al. (2010) and Norris et al. (2010c,a) extended this effort to more dwarfs and lower metallicities. Even from these earliest studies, it was clear that the UFDs are enhanced in α elements such as oxygen, magnesium, calcium, and silicon, and unusually deficient in neutron-capture elements including barium and strontium, as detailed further in Section 3.4.

3.1. The Mass-Metallicity Relation

A correlation between the stellar mass or luminosity of a galaxy and its mean metallicity has been known for decades (e.g., Tremonti et al. 2004, and references therein). Simon & Geha (2007) and Kirby et al. (2008) showed that such a relationship also exists even in the ultra-faint dwarf regime, more than five orders of magnitude in luminosity below the galaxies examined by Tremonti et al. Kirby et al. (2013b) carefully quantified the stellar mass-metallicity relation for Local Group dwarfs, demonstrating that a single relation holds for all types of dwarf galaxies throughout the Local Group:

$$[\text{Fe}/\text{H}] = (-1.68 \pm 0.03) + (0.29 \pm 0.02) \log \left(\frac{L_V}{10^6 L_\odot} \right), \quad 2.$$

with a standard deviation around the fit of only 0.16 dex. Including measurements made since 2013 for a larger sample of Milky Way satellites (see Figure 5), we find a best fit consistent with that reported by Kirby et al. (2013b), although with an increased intrinsic scatter of ~ 0.25 dex primarily attributable to the faintest dwarfs.

The existence of a tight correlation between luminosity and metallicity argues against severe tidal stripping of the stellar components of dwarf galaxies. Tidal stripping reduces the luminosity of a system without significantly changing its metallicity.⁸ Stripping will therefore tend to increase the scatter in the correlation; indeed, the two dwarfs known to be stripped because of the presence of substantial tidal tails, Sagittarius and Tuc III, lie ~ 0.8 dex and ~ 0.5 dex above the correlation. The fact that the correlation remains in place therefore puts an upper limit on the amount of stripping that could have occurred for the bulk of the dwarf galaxy population. However, since the dark matter halos of galaxies are much more extended than their stars, a large fraction of the dark matter in dSphs and UFDs could be removed without affecting the luminosity-metallicity relation.

The reader may observe that the scatter in the luminosity-metallicity relation appears to increase substantially for UFDs around $M_V \gtrsim -5.5$, and even more so at $M_V \gtrsim -4.0$. This increased dispersion could be interpreted as evidence that the faintest dwarfs have

⁸In the case of a metallicity gradient with the most metal-rich stars near the center of the galaxy, stripping would actually increase the overall metallicity slightly as low metallicity stars in the outskirts are preferentially stripped.

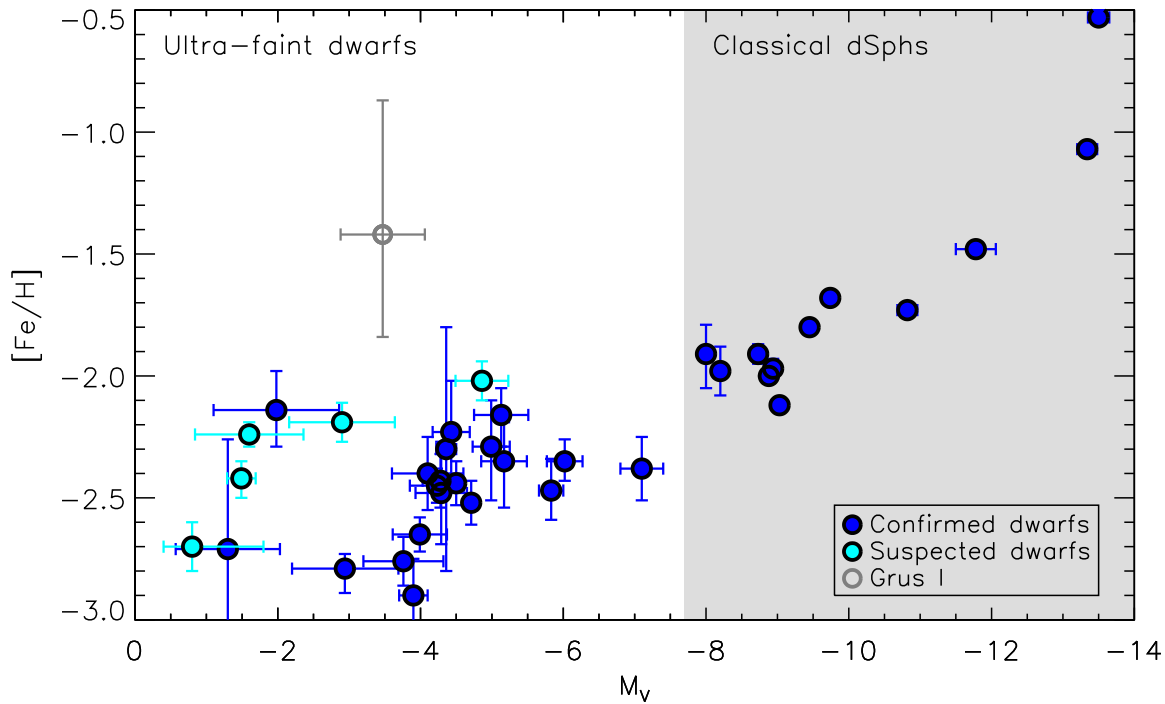


Figure 5 Mean stellar metallicities of Milky Way satellites as a function of absolute magnitude. Confirmed dwarf galaxies are displayed as dark blue filled circles, and objects suspected to be dwarf galaxies but for which the available data are not conclusive are shown as cyan filled circles. Grus I, for which there is no published classification, is shown as an open gray circle. The error bars in the vertical direction indicate the uncertainty on the mean metallicity of each object. The dwarf galaxy/candidate data included in this plot are listed in Table 1. The overall relationship between metallicity and luminosity is clear, although the scatter is large at the faint end.

suffered more stripping than the classical dSphs. Alternatively, (underestimated) observational uncertainties and errors may be responsible for some or all of the larger scatter at the lowest luminosities. In particular, the metallicities of some of the outliers above the relation are currently determined from only two member stars (e.g., Willman 1 and Tri II). If the brightest stars in those systems happen not to be representative of the overall metallicity distribution then the derived mean metallicity will be incorrect. The most significant outlier is Grus I, which is reported by Walker et al. (2016) to contain four stars (out of seven measured) with $[Fe/H] > -1.4$. No other UFD contains so many metal-rich stars, suggesting that some of them are probably foreground contaminants and that the system is actually more metal-poor.

3.2. Metallicity Distribution Functions

In contrast to the classical dSphs, relatively little work has been done on the metallicity distribution functions (MDFs) in ultra-faint dwarfs. This lack of attention is largely a result of the small samples of metallicity measurements typically available for UFDs. The best-studied object is Boo I, for which Norris et al. (2010b) derived an MDF with 16 stars and Lai et al. (2011) determined an MDF with 41 stars. The shape of the Boo I MDF is qualitatively similar to those obtained by Kirby et al. (2011) for the classical dSphs, although with a narrower peak. Kirby et al. (2008) showed that the combined MDF of seven UFDs and CVn I is very similar to the MDF of the Milky Way halo over the metallicity range from $[\text{Fe}/\text{H}] = -2$ to $[\text{Fe}/\text{H}] = -3.5$. Brown et al. (2014) determined MDFs for six UFDs, finding suggestions of multiple peaks in the metallicity distributions in several cases (most notably Boo I and Hercules). However, given the sparseness of the data for most galaxies, few authors have attempted to draw conclusions about the evolutionary history of UFDs from the observed MDFs (see Section 3.3). Lai et al. (2011) found that the Extra Gas model of Kirby et al. (2011) provides the best fit to the Boo I MDF, with most of the stars forming from an accreted reservoir of pristine gas, although the alternative Kirby et al. models (Pre-Enriched and Pristine) also fit the data acceptably well. The effective yield derived by Lai et al. (2011) for any of the three models continues the trend found by Kirby et al. (2011) of decreasing effective yield with decreasing stellar mass.

3.3. Chemical Evolution Histories

Beyond the MDF, the most basic feature of galactic chemical evolution is the dependence of the abundance of α elements on metallicity. At low metallicity, high $[\alpha/\text{Fe}]$ ratios are observed, while more metal-rich stars have low $[\alpha/\text{Fe}]$ ratios. This behavior results from the different chemical yields from different types of SNe. Core-collapse SNe from massive stars explode quickly after star formation occurs, producing large quantities of α elements. As time passes, Type Ia SNe begin to explode, producing primarily iron-peak elements and thereby lowering the $[\alpha/\text{Fe}]$ ratio (Tinsley 1979).

The timing of the transition between chemical enrichment dominated by core-collapse SNe and SNe Ia varies from galaxy to galaxy because it depends on the star formation rate (e.g., Venn et al. 2004; Kirby et al. 2011). In the compilation of 7 UFDs by Vargas et al. (2013), this transition appears to occur rather sharply at $[\text{Fe}/\text{H}] = -2.3$ when the data for the entire sample are combined. The observation of high $[\alpha/\text{Fe}]$ at $[\text{Fe}/\text{H}] < -2.3$ and \sim solar $[\alpha/\text{Fe}]$ at $[\text{Fe}/\text{H}] > -2.3$ is interpreted in the standard picture as evidence that Type Ia SNe began to contribute significantly to chemical enrichment at $[\text{Fe}/\text{H}] \approx -2.3$. In that case, star formation in UFDs must have continued for $\gtrsim 100$ Myr so that some SNe Ia exploded before the cessation of star formation (e.g., Vargas et al. 2013). However, Jeon, Besla & Bromm (2017) suggested instead that the lack of a clear knee in the $[\alpha/\text{Fe}]$ vs. $[\text{Fe}/\text{H}]$ diagram indicates that the UFDs were predominantly enriched by core-collapse SNe.

Only one galaxy, Segue 1, shows no evidence for a change in $[\alpha/\text{Fe}]$ over a broad range in metallicity (Vargas et al. 2013; Frebel, Simon & Kirby 2014). This abundance pattern is consistent with the one-shot enrichment scenario of Frebel & Bromm (2012, although see Webster, Frebel & Bland-Hawthorn 2016 for alternative possibilities), with star formation in Segue 1 likely lasting for less than a few hundred Myr and ending before any SNe Ia occurred.

Analytical chemical evolution models can provide insight into star formation and nucleosynthesis processes in galaxies (e.g., Searle & Sargent 1972, see Audouze & Tinsley 1976 and Nomoto, Kobayashi & Tominaga 2013 for reviews). Thus far, such models have only been applied to two UFDs, Hercules and Boo I (Vincenzo et al. 2014; Romano et al. 2015). By simultaneously fitting the observed stellar masses, MDFs, and $[\alpha/\text{Fe}]$ ratios, Vincenzo et al. (2014) showed that the UFDs formed with smaller gas reservoirs and star formation efficiencies a factor of ~ 10 lower than the classical dSphs. In agreement with previous results from the classical dSphs (e.g., Kirby, Martin & Finlator 2011), Vincenzo et al. (2014) found that most of the gas and metals are removed from the galaxies by galactic winds, although Romano et al. (2015) concluded that gas removal by tidal and ram-pressure stripping is more likely for Boo I. Extending these models to a larger sample of UFDs covering a wider range of parameter space would be very interesting, but requires increased numbers of metallicity and $[\alpha/\text{Fe}]$ measurements to be feasible.

Several recent numerical studies have explored the chemical evolution of UFD galaxies via hydrodynamic simulations. Using idealized models, Webster, Sutherland & Bland-Hawthorn (2014) and Bland-Hawthorn, Sutherland & Webster (2015) showed that dark matter halos as small as $10^7 M_{\odot}$ can retain gas after SN explosions, while less massive halos are evacuated after a single SN. They also found that only SNe near the center of a galaxy have a significant impact on its gas content; most of the energy from SNe that explode in the outskirts is lost to the intergalactic medium. In these models, the observed behavior of $[\alpha/\text{Fe}]$ as a function of metallicity from Vargas et al. (2013) can be reproduced if the duration of star formation is a few hundred Myr. Webster, Bland-Hawthorn & Sutherland (2015) extended this work by examining the effect of different star formation histories. They concluded that multiple well-separated bursts of star formation, as modeled by, e.g., Brown et al. (2014), produce more extremely metal-poor stars and fewer low $[\alpha/\text{Fe}]$ stars than observed. However, a model with continuous star formation (with brief pauses as the gas is heated by SNe) and ongoing self-enrichment provides a reasonable match to the data. More sophisticated simulations have been carried out by Jeon, Besla & Bromm (2017), who studied the formation of several UFDs in a cosmological context with a chemical reaction network. Jeon, Besla & Bromm (2017) demonstrated that a combination of reionization and SN feedback is necessary to quench star formation in these objects. Each of the dwarfs they simulated experienced several mergers at early times, with $\sim 10 - 20\%$ of the stars forming outside the main progenitor halo. In these models, the lowest metallicity UFD stars formed in halos that were enriched by Population III SN explosions in neighboring halos, while stars at $[\text{Fe}/\text{H}] \gtrsim -3$ primarily formed in situ with enrichment dominated by Population II SNe. As with the simpler models of Webster, Bland-Hawthorn & Sutherland (2015), the chemical abundances predicted by the Jeon, Besla & Bromm simulations ($[\text{C}/\text{Fe}]$ and $[\alpha/\text{Fe}]$) are in reasonable agreement with observed UFDs.

3.4. Chemical Abundance Patterns

Early studies of the detailed chemical abundance patterns of stars in UFDs focused on broad trends as a function of metallicity, which for the most part resemble the abundance trends of Milky Way halo stars in the same metallicity range (e.g., Koch et al. 2008; Frebel et al. 2010; Norris et al. 2010c,a). Ultra-faint dwarf stars are enhanced in α elements by ~ 0.3 dex, have Cr abundances that increase linearly with metallicity, are sometimes enhanced in carbon, and have low abundances of neutron-capture elements. Stars that are outliers from these

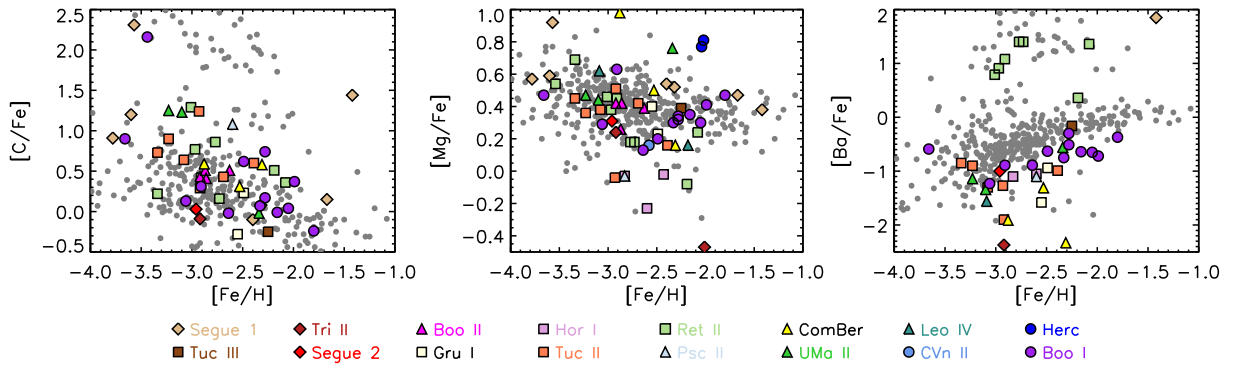


Figure 6 Chemical abundance patterns of stars in UFDs. The left, middle, and right panels show $[C/Fe]$, $[Mg/Fe]$, and $[Ba/Fe]$ ratios as a function of metallicity, respectively. UFD stars are plotted as colored diamonds, squares, triangles, and circles, as listed in the legend at bottom. The UFD data have been adopted from Koch et al. (2008), Feltzing et al. (2009), Frebel et al. (2010, 2016), Simon et al. (2010), Norris et al. (2010a,b,c), Lai et al. (2011), Gilmore et al. (2013), Koch et al. (2013), Frebel, Simon & Kirby (2014), Ishigaki et al. (2014), Roederer & Kirby (2014), Ji et al. (2016b,c), François et al. (2016), Kirby et al. (2017), Hansen et al. (2017), Nagasawa et al. (2018), Chiti et al. (2018), Spite et al. (2018), and Ji et al. (2018). A sample of metal-poor Milky Way halo stars from Cohen et al. (2013) and Roederer et al. (2014) is displayed as small gray circles for comparison.

general results in specific abundance ratios do exist, but their frequency does not seem to be high (e.g., Vargas et al. 2013).

3.4.1. Typical Ultra-Faint Dwarfs. Chemical abundance measurements from high-resolution spectroscopy are now available for at least one star in 16 UFDs. This sample currently contains more than 50 stars, with metallicities ranging from $[Fe/H] = -1.4$ to $[Fe/H] = -3.8$. With a handful of exceptions, the abundance patterns of different ultra-faint dwarfs closely resemble each other (see, e.g., Chiti et al. 2018), such that the galaxy in which a star is located cannot be discerned by examining its chemical abundances (see Figure 6). Some of the examples of distinct abundance patterns include the low $[\alpha/Fe]$ ratios in Horologium I (Nagasawa et al. 2018) and low $[Sc/Fe]$ ratios in Com Ber and possibly Segue 2 (Frebel et al. 2010; Roederer & Kirby 2014).

For elements through the iron peak, the abundances of ultra-faint dwarf stars closely follow the halo trend as a function of metallicity (Fig. 6). This result strongly suggests that nucleosynthesis and chemical evolution at early times do not depend significantly on galactic environment (e.g., Tolstoy, Hill & Tosi 2009; Simon et al. 2010). Whether the dispersion in abundance for each element at a constant metallicity matches between halo stars and the UFDs has not been investigated, but could be illuminating as to early chemical evolution and star formation. At the lowest metallicities, a significant fraction of UFD stars have high carbon abundances (e.g., Frebel et al. 2010; Norris et al. 2010a; Salvadori, Skúladóttir & Tolstoy 2015; Ji et al. 2016b; Spite et al. 2018), again matching previous findings for the

halo.

The only clear distinction between the abundance patterns of UFDs and halo stars is seen in the heaviest elements. For most UFD stars these measurements are limited to Ba and Sr, which have the strongest lines at optical wavelengths for typical enrichment levels. The UFD [Ba/Fe] and [Sr/Fe] abundance ratios are not usually outside the distribution of Ba and Sr abundances in the Milky Way halo, but most UFDs have abundance ratios that are significantly ($\gtrsim 1$ dex) lower than the average ratios for halo stars. Despite the much larger sample of halo stars available in the literature, some of the lowest Ba and Sr abundances ever measured are found in UFDs. Very low abundances of neutron-capture elements have been suggested as a possible characteristic for distinguishing UFDs from globular clusters in difficult cases (Ji et al. 2018); low aluminum abundances may also separate dwarfs from clusters.

3.4.2. Rare Enrichment Events in Ultra-Faint Dwarfs. Perhaps the biggest surprise from chemical abundance measurements in UFDs was the recent discovery of extreme enrichment of r-process elements in Reticulum II (Ji et al. 2016a; Roederer et al. 2016). Out of nine Ret II stars for which high-resolution spectra have been obtained, seven have [Eu/Fe] > 0.9 and [Ba/Fe] > 0.3 (Ji et al. 2016a). From the full sample of previously-studied ultra-faint dwarf stars, none have [Ba/Fe] > 0 and only one (an s-process-enhanced binary in Segue 1) has [Eu/Fe] > 0 . In fact, the Segue 1 binary, which was presumably contaminated with heavy elements by a companion that went through an AGB phase, was the only previous star in which Eu had been detected at all. Compared to most stars in UFDs, Ret II is enriched in Sr and Eu by a factor of > 30 , and in Ba by a factor of $\gtrsim 100$. As shown by Ji et al. (2016a,b) and Roederer et al. (2016), the abundance patterns of the Eu-rich stars in Ret II perfectly match the r-process enrichment pattern seen in r-process-enhanced Milky Way stars and the Sun.

The only viable explanation for the chemical abundances of Ret II is that a single nucleosynthetic event early in the history of the galaxy produced a large quantity of r-process material ($\sim 10^{-5} M_{\odot}$ of Eu; Ji et al. 2016a). Given that nine other UFDs had been observed prior to Ret II, and no sign of significant r-process enrichment was detected in any of them, whatever produced the neutron-capture elements in Ret II must have been a rare occurrence. Ret II does not have a large stellar mass among UFDs, so it is very unlikely that an event would take place multiple times in Ret II and never in any other similar galaxies. Therefore, the very large overabundance of r-process elements also indicates that this single event must have produced copious amounts of such elements. Ordinary SNe do not have these characteristics, leaving a neutron star merger or a magneto-rotationally driven SN as the possible sites for r-process nucleosynthesis in Ret II (Ji et al. 2016a; Roederer et al. 2016). As a result of the observational evidence for r-process nucleosynthesis by the neutron star merger GW170817 (e.g., Chornock et al. 2017; Cowperthwaite et al. 2017; Drout et al. 2017; Kasliwal et al. 2017; Pian et al. 2017; Shappee et al. 2017; Smartt et al. 2017), as well as the approximate agreement in the inferred rates of such events, a neutron star merger is heavily favored as the primary origin of r-process elements in Ret II and other dwarf galaxies.

Subsequent to the identification of Ret II as an r-process-rich galaxy, Hansen et al. (2017) showed that the brightest star in Tuc III is also enhanced in r-process elements. The rate of r-process enhancement in UFDs can therefore be updated to two out of 14 galaxies. The r-process abundances in Tuc III are significantly lower than in Ret II, but

still well above those in any other UFD. This abundance pattern implies that either the nucleosynthetic event in Tuc III produced less r-process material, it was diluted into a larger mass of gas, or that a larger fraction of the r-process yield of the event escaped the galaxy.

Although the abundance of r-process elements in other ultra-faint dwarfs is several orders of magnitude lower than in Ret II and Tuc III, those elements are still detected at very low levels in almost every galaxy for which sufficient data exist (e.g., Frebel et al. 2010; Roederer 2013; Gilmore et al. 2013; Frebel, Simon & Kirby 2014; Ishigaki et al. 2014; Chiti et al. 2018). If Ret II was enriched by a single r-process event, then the only way the same mechanism could account for much lower — but nonzero — r-process abundances in other UFDs is if the gas masses of those systems were much larger than in Ret II or the retention fraction of r-process ejecta were much lower. Straightforward calculations indicate that these possibilities are unlikely (see below). Therefore, the natural conclusion is that a second site of r-process nucleosynthesis exists, which produces much smaller amounts of r-process material (Ji et al. 2016b). This alternate pathway of creating heavy elements can likely be identified with core-collapse SNe (e.g., Lee et al. 2013).

Theoretical modeling of the r-process enrichment of UFDs is still in its early stages. However, the work that has been done from several different directions confirms that the scenario proposed by Ji et al. (2016a) is both physically plausible and can quantitatively explain the observed r-process abundances. Specifically, Beniamini, Hotokezaka & Piran (2016a,b) and Beniamini, Dvorkin & Silk (2018) used analytical calculations to demonstrate that (1) binary neutron stars can be retained in low-mass dwarfs despite possible SN kicks, (2) a non-negligible fraction of such binaries will merge in less than ~ 100 Myr, (3) each nucleosynthesis event must produce $\sim 10^{-5} M_{\odot}$ of Eu and occur at a rate of one per ~ 2000 SNe, (4) up to $\sim 90\%$ of the r-process material synthesized should remain in the galaxy, and (5) $\sim 7\%$ of UFDs should be enriched by an r-process event. Chemical evolution modeling by Komiya & Shigeyama (2016) showed that r-process synthesis by neutron star mergers can also reproduce the distribution of [Eu/Fe] and [Ba/Fe] abundance ratios for metal-poor stars in the Milky Way halo, under the assumptions of a lower star formation efficiency in dwarf galaxies and a size-dependent escape fraction for r-process material. Hydrodynamic simulations of UFDs by Safarzadeh & Scannapieco (2017) also support this picture, showing that a neutron star merger near the center of Ret II can reasonably account for the observed distribution of [Eu/H] and [Fe/H] values. If the merger occurred in the outskirts of the galaxy, on the other hand, lower Eu abundances that are uncorrelated with metallicity would be expected.

Table 1. Dwarf Galaxy Data

Dwarf	M_V	$R_{1/2}$ (pc)	Distance (kpc)	v_{hel} (km s^{-1})	σ (km s^{-1})	[Fe/H]	$\sigma_{[\text{Fe}/\text{H}]}$	References ^{a,b}
Tucana IV	$-3.50^{+0.28}_{-0.28}$	127^{+26}_{-22}	$48.0^{+4.0}_{-4.0}$					1,1,1, γ,γ,γ
Sculptor	$-10.82^{+0.14}_{-0.14}$	279^{+16}_{-16}	$86.0^{+5.0}_{-5.0}$	$111.4^{+0.1}_{-0.1}$	$9.2^{+1.1}_{-1.1}$	$-1.73^{+0.03}_{-0.02}$	$0.44^{+0.02}_{-0.02}$	2,2,3,4,5,6,6
Cetus II	$0.00^{+0.68}_{-0.68}$	17^{+9}_{-5}	$30.0^{+3.0}_{-3.0}$					1,1,1, γ,γ,γ
Cetus III	$-2.45^{+0.57}_{-0.56}$	90^{+32}_{-14}	$251.0^{+24.0}_{-11.0}$					7,7,7, γ,γ,γ
Triangulum II	$-1.60^{+0.76}_{-0.76}$	16^{+4}_{-4}	$28.4^{+1.6}_{-1.6}$		$< 3.4^c$	$-2.24^{+0.05}_{-0.05}$	$0.53^{+0.12}_{-0.38}$	2,2,8,9,9,9,9
Segue 2	$-1.98^{+0.88}_{-0.88}$	40^{+4}_{-4}	$37.0^{+3.0}_{-3.0}$	$-381.7^{+1.1}_{-1.1}$	$< 2.2^c$	$-2.14^{+0.16}_{-0.13}$	$0.39^{+0.12}_{-0.13}$	2,2,10,11,11,6,6
DESJ0225+0304	$-1.10^{+0.50}_{-0.30}$	19^{+9}_{-5}	$23.8^{+0.7}_{-0.5}$	$-40.2^{+0.9}_{-0.9}$				12,12,12, γ,γ,γ
Hydrus I	$-4.71^{+0.08}_{-0.08}$	53^{+4}_{-4}	$27.6^{+0.5}_{-0.5}$	$80.4^{+0.6}_{-0.6}$	$2.7^{+0.5}_{-0.4}$	$-2.52^{+0.09}_{-0.09}$	$0.41^{+0.08}_{-0.08}$	13,13,13,13,13,13,13
Fornax	$-13.34^{+0.14}_{-0.14}$	792^{+18}_{-18}	$139.0^{+3.0}_{-3.0}$	$55.2^{+0.1}_{-0.1}$	$11.7^{+0.9}_{-0.9}$	$-1.07^{+0.02}_{-0.01}$	$0.27^{+0.01}_{-0.01}$	2,14,15,4,5,6,6
Horologium I	$-3.76^{+0.56}_{-0.56}$	40^{+10}_{-9}	$87.0^{+13.0}_{-11.0}$	$112.8^{+2.5}_{-2.6}$	$4.9^{+2.8}_{-0.9}$	$-2.76^{+0.10}_{-0.10}$	$0.17^{+0.20}_{-0.03}$	2,2,16,17,18,18,18
Horologium II	$-1.56^{+1.02}_{-1.02}$	44^{+15}_{-14}	$78.0^{+8.0}_{-7.0}$					2,2,19, γ,γ,γ
Reticulum II	$-3.99^{+0.38}_{-0.38}$	51^{+3}_{-3}	$31.6^{+1.5}_{-1.4}$	$62.8^{+0.5}_{-0.5}$	$3.3^{+0.7}_{-0.7}$	$-2.65^{+0.07}_{-0.07}$	$0.28^{+0.09}_{-0.09}$	2,2,20,21,21,21,21
Eridanus II	$-7.10^{+0.30}_{-0.30}$	246^{+17}_{-17}	$366.0^{+17.0}_{-17.0}$	$75.6^{+1.3}_{-1.3}$	$6.9^{+1.2}_{-0.9}$	$-2.38^{+0.13}_{-0.13}$	$0.47^{+0.12}_{-0.09}$	22,22,22,23,23,23,23
Reticulum III	$-3.30^{+0.29}_{-0.29}$	64^{+26}_{-23}	$92.0^{+13.0}_{-13.0}$					1,1,1, γ,γ,γ
Pictor I	$-3.67^{+0.60}_{-0.60}$	32^{+15}_{-15}	$126.0^{+19.0}_{-16.0}$					2,2,16, γ,γ,γ
Columba I	$-4.20^{+0.20}_{-0.20}$	117^{+12}_{-12}	$183.0^{+10.0}_{-10.0}$					8,8,8, γ,γ,γ
Carina	$-9.45^{+0.05}_{-0.05}$	311^{+15}_{-15}	$106.0^{+5.0}_{-5.0}$	$222.9^{+0.1}_{-0.1}$	$6.6^{+1.2}_{-1.2}$	$-1.80^{+0.02}_{-0.02}$	0.24^d	2,2,24,4,5,25,25
Pictor II	$-3.20^{+0.40}_{-0.50}$	47^{+20}_{-13}	$45.0^{+5.0}_{-4.0}$					26,26,26, γ,γ,γ
Carina II	$-4.50^{+0.10}_{-0.10}$	92^{+8}_{-8}	$36.2^{+0.6}_{-0.6}$	$477.2^{+1.2}_{-1.2}$	$3.4^{+1.2}_{-0.8}$	$-2.44^{+0.09}_{-0.09}$	$0.22^{+0.10}_{-0.07}$	27,27,27,28,28,28,28
Carina III	$-2.40^{+0.20}_{-0.20}$	30^{+8}_{-8}	$27.8^{+0.6}_{-0.6}$	$284.6^{+3.4}_{-3.1}$	$5.6^{+4.3}_{-2.1}$			27,27,27,28,28, γ,γ
Ursa Major II	$-4.43^{+0.26}_{-0.26}$	139^{+9}_{-9}	$34.7^{+2.0}_{-1.9}$	$-116.5^{+1.9}_{-1.9}$	$5.6^{+1.4}_{-1.4}$	$-2.23^{+0.21}_{-0.24}$	$0.67^{+0.20}_{-0.15}$	2,2,29,30,31,6,6
Leo T	-8.00^e	118^{+11}_{-11}	$409.0^{+29.0}_{-27.0}$	$38.1^{+2.0}_{-2.0}$	$7.5^{+1.6}_{-1.6}$	$-1.91^{+0.12}_{-0.14}$	$0.43^{+0.13}_{-0.09}$	32,32,33,30,30,6,6
Segue 1	$-1.30^{+0.73}_{-0.73}$	24^{+4}_{-4}	$23.0^{+2.0}_{-2.0}$	$208.5^{+0.9}_{-0.9}$	$3.7^{+1.4}_{-1.1}$	$-2.71^{+0.45}_{-0.39}$	$0.99^{+0.42}_{-0.26}$	2,2,34,35,35,36,36

Table 1 (cont'd)

Dwarf	M_V	$R_{1/2}$ (pc)	Distance (kpc)	v_{hel} (km s^{-1})	σ (km s^{-1})	[Fe/H]	$\sigma_{[\text{Fe}/\text{H}]}$	References ^{a,b}
Leo I	$-11.78^{+0.28}_{-0.28}$	270^{+17}_{-16}	$254.0^{+16.0}_{-15.0}$	$282.9^{+0.5}_{-0.5}$	$9.2^{+0.4}_{-0.4}$	$-1.48^{+0.02}_{-0.01}$	$0.26^{+0.01}_{-0.01}$	2,2,37,38,38,6,6
Sextans	$-8.94^{+0.06}_{-0.06}$	456^{+15}_{-15}	$95.0^{+3.0}_{-3.0}$	$224.3^{+0.1}_{-0.1}$	$7.9^{+1.3}_{-1.3}$	$-1.97^{+0.04}_{-0.04}$	$0.38^{+0.03}_{-0.03}$	2,2,39,4,5,6,6
Ursa Major I	$-5.13^{+0.38}_{-0.38}$	295^{+28}_{-28}	$97.3^{+5.7}_{-5.7}$	$-55.3^{+1.4}_{-1.4}$	$7.0^{+1.0}_{-1.0}$	$-2.16^{+0.11}_{-0.13}$	$0.62^{+0.10}_{-0.08}$	2,40,41,30,31,6,6
Willman 1	$-2.90^{+0.74}_{-0.74}$	33^{+8}_{-8}	$45.0^{+10.0}_{-10.0}$	$-14.1^{+1.0}_{-0.8}$	$4.0^{+0.8}_{-0.8}$	$-2.19^{+0.08}_{-0.08}$		2,2,42,43,43,43,-
Leo II	$-9.74^{+0.04}_{-0.04}$	171^{+10}_{-10}	$233.0^{+14.0}_{-14.0}$	$78.3^{+0.6}_{-0.6}$	$7.4^{+0.4}_{-0.4}$	$-1.68^{+0.02}_{-0.03}$	$0.34^{+0.02}_{-0.02}$	2,2,44,45,45,6,6
Leo V	$-4.29^{+0.36}_{-0.36}$	49^{+16}_{-16}	$169.0^{+4.0}_{-5.0}$	$170.9^{+2.1}_{-1.9}$	$2.3^{+3.2}_{-1.6}$	$-2.48^{+0.23}_{-0.21}$	$0.47^{+0.23}_{-0.13}$	2,2,46,47,47,47,47
Leo IV	$-4.99^{+0.26}_{-0.26}$	114^{+13}_{-13}	$154.0^{+5.0}_{-5.0}$	$132.3^{+1.4}_{-1.4}$	$3.3^{+1.7}_{-1.7}$	$-2.29^{+0.19}_{-0.22}$	$0.56^{+0.19}_{-0.14}$	2,2,48,30,30,6,6
Crater II	$-8.20^{+0.10}_{-0.10}$	1066^{+86}_{-86}	$117.5^{+1.1}_{-1.1}$	$87.5^{+0.4}_{-0.4}$	$2.7^{+0.3}_{-0.3}$	$-1.98^{+0.04}_{-0.10}$	$0.22^{+0.04}_{-0.03}$	49,49,49,50,50,50,50
Virgo I	$-0.80^{+0.90}_{-0.90}$	38^{+12}_{-11}	$87.0^{+13.0}_{-8.0}$					51,51,51,-,-,-,-,-
Hydra II	$-4.86^{+0.37}_{-0.37}$	67^{+13}_{-13}	$151.0^{+5.0}_{-7.0}$	$303.1^{+1.4}_{-1.4}$	$< 3.6^c$	$-2.02^{+0.08}_{-0.08}$	$0.40^{+0.48}_{-0.26}$	2,2,52,53,53,53,53
Coma Berenices	$-4.28^{+0.25}_{-0.25}$	69^{+5}_{-4}	$42.0^{+1.6}_{-1.5}$	$98.1^{+0.9}_{-0.8}$	$4.6^{+0.8}_{-0.8}$	$-2.43^{+0.11}_{-0.11}$	$0.46^{+0.09}_{-0.08}$	2,2,54,30,30,6,6
Canes Venatici II	$-5.17^{+0.32}_{-0.32}$	71^{+11}_{-11}	$160.0^{+4.0}_{-4.0}$	$-128.9^{+1.2}_{-1.2}$	$4.6^{+1.0}_{-1.0}$	$-2.35^{+0.16}_{-0.19}$	$0.57^{+0.15}_{-0.12}$	2,2,55,30,30,6,6
Canes Venatici I	$-8.73^{+0.06}_{-0.06}$	437^{+18}_{-18}	$211.0^{+6.0}_{-6.0}$	$30.9^{+0.6}_{-0.6}$	$7.6^{+0.4}_{-0.4}$	$-1.91^{+0.04}_{-0.04}$	$0.39^{+0.03}_{-0.02}$	2,2,56,30,30,6,6
Boötes II	$-2.94^{+0.74}_{-0.74}$	39^{+5}_{-5}	$42.0^{+1.0}_{-1.0}$	$-117.0^{+5.2}_{-5.2}$	$10.5^{+7.4}_{-7.4}$	$-2.79^{+0.06}_{-0.10}$	$< 0.35^c$	2,2,57,58,58,59,59
Boötes I	$-6.02^{+0.25}_{-0.25}$	191^{+8}_{-8}	$66.0^{+2.0}_{-2.0}$	$101.8^{+0.7}_{-0.6}$	$4.6^{+0.8}_{-0.6}$	$-2.35^{+0.09}_{-0.08}$	$0.44^{+0.07}_{-0.06}$	2,2,60,61,61,62,62
Ursa Minor	$-9.03^{+0.05}_{-0.05}$	405^{+21}_{-21}	$76.0^{+4.0}_{-4.0}$	$-247.2^{+0.8}_{-0.8}$	$9.5^{+1.2}_{-1.2}$	$-2.12^{+0.03}_{-0.02}$	$0.33^{+0.02}_{-0.03}$	2,2,63,64,4,6,6
Draco II	$-0.80^{+0.40}_{-1.00}$	19^{+4}_{-3}	$21.5^{+0.4}_{-0.4}$	$-342.5^{+1.1}_{-1.2}$	$< 5.9^c$	$-2.70^{+0.10}_{-0.10}$	$< 0.24^c$	65,65,65,65,65,65,65
Hercules	$-5.83^{+0.17}_{-0.17}$	216^{+20}_{-20}	$132.0^{+6.0}_{-6.0}$	$45.0^{+1.1}_{-1.1}$	$5.1^{+0.9}_{-0.9}$	$-2.47^{+0.11}_{-0.12}$	$0.47^{+0.11}_{-0.08}$	2,2,66,30,30,6,6
Draco	$-8.88^{+0.05}_{-0.05}$	231^{+17}_{-17}	$82.0^{+6.0}_{-6.0}$	$-290.7^{+0.7}_{-0.8}$	$9.1^{+1.2}_{-1.2}$	$-2.00^{+0.02}_{-0.02}$	$0.34^{+0.02}_{-0.02}$	2,2,67,64,4,6,6
Sagittarius	$-13.50^{+0.15}_{-0.15}$	2662^{+193}_{-193}	$26.7^{+1.3}_{-1.3}$	$139.4^{+0.6}_{-0.6}$	$9.6^{+0.4}_{-0.4}$	$-0.53^{+0.03}_{-0.02}$	$0.17^{+0.02}_{-0.02}$	68,68,69,70,70,71,71
Sagittarius II	$-5.20^{+0.10}_{-0.10}$	33^{+2}_{-2}	$70.1^{+2.3}_{-2.3}$					20,20,20,-,-,-,-,-
Indus II	$-4.30^{+0.19}_{-0.19}$	181^{+70}_{-64}	$214.0^{+16.0}_{-16.0}$					1,1,1,-,-,-,-,-
Grus II	$-3.90^{+0.22}_{-0.22}$	93^{+16}_{-12}	$53.0^{+5.0}_{-5.0}$					1,1,1,-,-,-,-,-

Table 1 (cont'd)

Dwarf	M_V	$R_{1/2}$ (pc)	Distance (kpc)	v_{hel} (km s $^{-1}$)	σ (km s $^{-1}$)	[Fe/H]	$\sigma_{[\text{Fe}/\text{H}]}$	References ^{a,b}
Pegasus III	$-4.10^{+0.50}_{-0.50}$	78^{+31}_{-25}	$205.0^{+20.0}_{-20.0}$	$-222.9^{+2.6}_{-2.6}$	$5.4^{+3.0}_{-2.5}$	$-2.40^{+0.15}_{-0.15}$		72, 72, 72, 73, 73, 73, -
Aquarius II	$-4.36^{+0.14}_{-0.14}$	160^{+26}_{-26}	$107.9^{+3.3}_{-3.3}$	$-71.1^{+2.5}_{-2.5}$	$5.4^{+3.4}_{-2.5}$	$-2.30^{+0.50}_{-0.50}$		74, 74, 74, 74, 74, 49, -
Tucana II	$-3.90^{+0.20}_{-0.20}$	121^{+35}_{-35}	$58.0^{+8.0}_{-8.0}$	$-129.1^{+3.5}_{-3.5}$	$8.6^{+4.4}_{-3.5}$	$-2.90^{+0.15}_{-0.15}$	$0.29^{+0.15}_{-0.15}$	16, 16, 16, 16, 75, 75, 76, 76
Grus I	$-3.47^{+0.59}_{-0.59}$	28^{+23}_{-23}	$120.0^{+12.0}_{-12.0}$	$-140.5^{+2.4}_{-2.4}$	$2.9^{+2.1}_{-2.1}$	$-1.42^{+0.55}_{-0.42}$	$0.41^{+0.42}_{-0.33}$	2, 2, 17, 75, 75, 75, 75, 75
Pisces II	$-4.23^{+0.38}_{-0.38}$	60^{+10}_{-10}	$183.0^{+15.0}_{-15.0}$	$-226.5^{+2.7}_{-2.7}$	$5.4^{+3.6}_{-2.4}$	$-2.45^{+0.07}_{-0.07}$	$0.48^{+0.70}_{-0.29}$	2, 2, 77, 53, 53, 53, 53, 53
Tucana V	$-1.60^{+0.49}_{-0.49}$	16^{+5}_{-5}	$55.0^{+9.0}_{-9.0}$					1, 1, 1, -, -, -, -, -
Phoenix II	$-2.70^{+0.40}_{-0.40}$	37^{+8}_{-8}	$84.3^{+4.0}_{-4.0}$					20, 20, 20, -, -, -, -
Tucana III	$-1.49^{+0.20}_{-0.20}$	37^{+9}_{-9}	$25.0^{+2.0}_{-2.0}$	$-102.3^{+0.4}_{-0.4}$	$< 1.2^c$	$-2.42^{+0.07}_{-0.08}$	$< 0.19^c$	20, 20, 1, 78, 78, 78, 78, 78

Note. — These data are provided as a convenience to the community. However, in recognition of the effort invested by many researchers to obtain, reduce, analyze, and publish these measurements, we strongly encourage authors to cite the original references (which are listed below), not just this compilation, where possible.

^aReferences: (1) Drllica-Wagner et al. (2015); (2) Muñoz et al. (2018); (3) Pietrzyński et al. (2008); (4) Walker et al. (2009a); (5) Walker, Mateo & Olszewski (2009); (6) Kirby et al. (2013b); (7) Homma et al. (2013); (8) Carlin et al. (2017); (9) Kirby et al. (2017); (10) Boettcher et al. (2013); (11) Kirby et al. (2013a); (12) Luque et al. (2017); (13) Kopusov et al. (2018); (14) Battaglia et al. (2006); (15) Rizzi et al. (2007); (16) Bechtol et al. (2015); (17) Kopusov et al. (2015a); (18) Kopusov et al. (2015b); (19) Kim & Jerjen (2015); (20) Muthu-Pakdil et al. (2018); (21) Simon et al. (2015); (22) Crnojević et al. (2016a); (23) Li et al. (2017); (24) Karczarek et al. (2015); (25) Fabrizio et al. (2012); (26) Drllica-Wagner et al. (2016); (27) Torrealba et al. (2018); (28) Li et al. (2018b); (29) Dall’Ora et al. (2012); (30) Simon & Geha (2007); (31) this work (32) de Jong et al. (2008); (33) Clementini et al. (2012); (34) Belokurov et al. (2007); (35) Simon et al. (2011); (36) Frebel, Simon & Kirby (2014); (37) Bellazzini et al. (2004); (38) Mateo, Olszewski & Walker (2008); (39) Lee et al. (2003); (40) Okamoto et al. (2008); (41) Garofalo et al. (2013); (42) Willman et al. (2005a); (43) Willman et al. (2011); (44) Bellazzini, Gennari & Ferraro (2005); (45) Spencer et al. (2017); (46) Medina et al. (2018); (47) Collins et al. (2017); (48) Moretti et al. (2009); (49) Torrealba et al. (2016a); (50) Caldwell et al. (2017); (51) Homma et al. (2016); (52) Vivas et al. (2016); (53) Kirby, Simon & Cohen (2015); (54) Musella et al. (2009); (55) Greco et al. (2008); (56) Kuehn et al. (2008); (57) Walsh et al. (2008); (58) Koch et al. (2009); (59) Ji et al. (2016c); (60) Dall’Ora et al. (2006); (61) Kopusov et al. (2011); (62) Brown et al. (2014); (63) Bellazzini et al. (2002); (64) Muñoz et al. (2005); (65) Longeard et al. (2018); (66) Musella et al. (2012); (67) Kinemuchi et al. (2008); (68) Majewski et al. (2003); (69) Hamañowicz et al. (2016); (70) Bellazzini et al. (2008); (71) Mucciarelli et al. (2017); (72) Kim et al. (2015a); (73) Kim et al. (2016); (74) Torrealba et al. (2016b); (75) Walker et al. (2016); (76) Chiti et al. (2018); (77) Sand et al. (2012); (78) Simon et al. (2017).

^bThe references listed for each object are for, in order: (1) M_V , (2) $R_{1/2}$, (3) distance, (4) v_{hel} , (5) σ , (6) [Fe/H], and (7) $\sigma_{[\text{Fe}/\text{H}]}$. Inasmuch as the properties of some galaxies have been determined by multiple studies, this reference list is not intended to be complete. Instead, it represents our assessment of the best available data. In cases where no velocity and/or metallicity measurements are available in the literature, a dash is listed in place of the corresponding reference.

^cUpper limits are at 90% confidence. Where the original reference does not provide a value at that confidence interval, we have determined one from the data.

^dNo uncertainty on the metallicity dispersion of Carina was provided by Fabrizio et al. (2012).

4. STRUCTURAL PROPERTIES

A homogeneous analysis of the structural properties of the early SDSS UFDs was provided by Martin, de Jong & Rix (2008). Muñoz et al. (2018) recently updated this work, presenting uniform processing of deep photometry for all UFDs known as of mid-2015 (of course, a number of new dwarfs have been discovered since that date). Many previous studies have shown that the radial profiles of ultra-faint dwarfs can be accurately described by either exponential or Plummer (1911) profiles⁹ (e.g., Belokurov et al. 2006; Martin, de Jong & Rix 2008; Sand et al. 2010). Muñoz et al. (2018) advocated instead for Sérsic profiles, which match the observed radial profiles more closely (and are widely used for brighter galaxies), at the cost of one additional degree of freedom in the fit. Confirmed UFDs have half-light radii ranging from 24 pc (Segue 1) to 295 pc (UMa I), with candidate UFDs extending down to 15 – 20 pc in a few cases. In comparison, the classical dSphs have half-light radii between 170 pc (Leo II) and 2660 pc (Sagittarius).

Apart from simply being smaller on average, it has also been suggested that the faintest galaxies have significantly larger ellipticities than larger systems (Martin, de Jong & Rix 2008). Updating the samples from what was available ten years ago, we calculate a weighted average ellipticity for the UFDs of 0.50 ± 0.01 , while the weighted average ellipticity of the classical dSphs is 0.350 ± 0.003 , in good agreement with the statistics determined by Martin, de Jong & Rix (2008). However, using a two-sided Kolmogorov-Smirnov test we find that there is a 19% probability that the two samples are drawn from a common distribution (as previously indicated by Sand et al. 2012). We therefore conclude that there is no significant evidence at present that UFDs have more elongated shapes than more luminous dwarfs.

A recurring question regarding the structure of the faintest dwarfs is whether their isophotes are irregular or distorted in any way, which could suggest recent tidal stripping (e.g., Zucker et al. 2006a; Belokurov et al. 2006; Okamoto et al. 2012). Several analyses of simulated photometric data sets of faint dwarfs have shown that these apparently irregular shapes are the result of Poisson fluctuations in the distribution of stars in the lowest surface brightness regions of these systems rather than evidence for disturbed morphology (Walsh et al. 2008; Martin, de Jong & Rix 2008; Muñoz, Geha & Willman 2010).

The recent discovery of the relatively luminous ($M_V = -8.2$), but extremely diffuse, Crater II dwarf (Torrealba et al. 2016a) highlights the possibility that the currently known population of dwarf galaxies may be limited in surface brightness by the sensitivity of existing photometric surveys. Indeed, Muñoz et al. (2018) clearly illustrate how the discovery of new Milky Way satellites has pushed to lower and lower surface brightnesses as the available data have improved. There are also theoretical reasons to suspect that significant numbers of even lower surface brightness dwarfs could exist (e.g., Bullock et al. 2010). In the next decade, LSST observations will reveal whether there is a large population of even feebler dwarf galaxies, or if we have already reached the lowest surface brightness at which galaxies are able to form.

5. STELLAR POPULATIONS AND GAS CONTENT

The gold standard for determining star formation histories based on resolved stellar populations is *Hubble Space Telescope* (HST) photometry, because of its superior photometric

⁹As discussed in Section 2.1.3, the only UFD for which these profiles do not fit is UMa II (Muñoz, Geha & Willman 2010; Muñoz et al. 2018).

accuracy and stability relative to ground-based data. One challenge facing such work for UFDs is small-number statistics. Obtaining strong constraints on the star formation history of an old stellar population requires a sample of at least $\sim 200 - 300$ stars near the main sequence turnoff (Brown et al. 2014). The lowest-luminosity dwarfs simply do not contain enough stars to meet this criterion even if every star in the galaxy is observed. Accurate star formation histories can be obtained for systems with absolute magnitudes brighter than $M_V \approx -3$, although doing so may require a number of HST pointings in order to include as many stars as possible. HST-based star formation histories have been published for 6 UFDs.

5.1. Star Formation Histories

The first analysis of deep HST imaging of UFDs was carried out by Brown et al. (2012), studying Hercules, Leo IV, and UMa I. They concluded that the three galaxies have similar ages, and are each as old or older than the prototypical ancient globular cluster M92. Brown et al. (2014) expanded the sample to six UFDs, adding Boo I, Canes Venatici II (CVn II), and Coma Berenices (Com Ber) to the previous three. By incorporating improved spectroscopic MDFs and updated isochrones matched to observed dwarf galaxy chemical abundance patterns, Brown et al. (2014) determined that all of the galaxies except UMa I had formed more than 75% of their stars by $z \sim 10$. Using a star formation model consisting of two bursts, the best fit for UMa I has approximately half of its stars forming at $z \sim 3$. A large majority of the stars in all six dwarfs had formed by the end of reionization at $z \sim 6$, consistent with the idea that gas heating by reionization ended star formation in such objects (e.g., Bullock, Kravtsov & Weinberg 2000; Somerville 2002; Benson et al. 2002). Note, however, that quenching by reionization does not necessarily mean that star formation ends precisely at the redshift of reionization, since sufficiently high-density molecular gas can survive somewhat beyond reionization even in low-mass halos (e.g., Oñorbe et al. 2015). Star formation histories have also been derived for Hercules, Leo IV, and CVn II by Weisz et al. (2014) from shallower WFPC2 data. Weisz et al. found that $> 90\%$ of the stars in Hercules and Leo IV are older than 11 Gyr, consistent with the Brown et al. (2014) results. In CVn II, however, Weisz et al. concluded that star formation continued until ~ 8 Gyr ago, in conflict with Brown et al. The reason for this discrepancy is not clear. Age estimates based on deep ground-based imaging are generally consistent with the HST results, although the constraints are not as tight (e.g., Sand et al. 2010; Okamoto et al. 2012).

Based on the available data, it appears likely that UFDs are uniformly ancient, with all or nearly all of their stars forming in the early universe. While most or all UFDs exhibit a blue plume of stars brighter than the main sequence turnoff, this population is best interpreted as blue stragglers rather than young stars (Santana et al. 2013). These objects can thus be considered pristine fossils from the era of reionization (e.g., Bovill & Ricotti 2009, 2011; Salvadori & Ferrara 2009). Improved age measurements to reveal how synchronized the star formation in such galaxies was would be very interesting. Conversely, a clear detection of younger stars in very low-luminosity dwarfs would have important implications for star formation in low-mass dark matter halos and perhaps for cosmology as well (e.g., Bozek et al. 2018).

5.2. Initial Mass Functions

Their low metallicities make UFDs some of the most extreme environments in which star formation is known to have occurred. They therefore present an promising opportunity to investigate how the stellar initial mass function (IMF) depends on galactic environment. Dwarf galaxies also offer the advantage that their low stellar densities mean that no dynamical evolution has occurred, unlike in globular clusters, so the present-day mass function can be assumed to match the initial one below the main sequence turnoff. Geha et al. (2013) measured the IMF in two ultra-faint dwarfs, Hercules and Leo IV, using star counts from the HST photometry of Brown et al. (2012). Over the mass range from $\sim 0.5 - 0.8 M_{\odot}$, they found that the best fitting power law had a slope of $\alpha \approx 1.2$, much shallower than the Salpeter (1955) value of $\alpha = 2.35$. While the uncertainties for Leo IV are quite large, in Hercules the slope disagrees with a Salpeter IMF at 5.8σ .

Intriguingly, such a bottom-light IMF in the least massive, lowest metallicity galaxies known suggests the possibility of a monotonic trend in IMF slope with galaxy properties. The largest elliptical galaxies have bottom-heavy IMFs (e.g., van Dokkum & Conroy 2010; Spiniello et al. 2012), and dwarf galaxies in the Local Group appear to exhibit increasingly shallower IMF slopes toward lower masses (Geha et al. 2013).

More recent analyses have complicated this picture. Gennaro et al. (2018b) measured the IMFs for the full sample of 6 UFDs from Brown et al. (2014), confirming that each galaxy has an IMF slope shallower than Salpeter when fit with a power law. However, when describing the IMF as a log-normal function (Chabrier 2003), the parameters for the UFDs are consistent with the Milky Way IMF. Gennaro et al. (2018a) used deeper, near-infrared imaging of Com Ber with HST to probe the IMF down to masses of $\sim 0.2 M_{\odot}$, comparable to the characteristic mass in the log-normal description of the Milky Way IMF. The results are consistent both with the shallower optical observations of Com Ber and the Chabrier (2003) Galactic IMF. These findings suggest that there may be significant IMF variations even within the class of UFDs, with some galaxies having shallow IMFs and others that resemble the Milky Way despite their low metallicities (Gennaro et al. 2018a).

If the IMF is indeed bottom-light in UFDs, there would be important implications for SN rates, feedback, chemical enrichment, and gas loss in such systems. A bottom-light IMF extrapolated to higher masses is top-heavy, which would produce larger numbers of SN explosions for a given mass of stars (of course, the validity of such an extrapolation is only an assumption, since no stars heavier than $\sim 0.8 M_{\odot}$ exist in UFDs today). This effect can be dramatic; Frebel, Simon & Kirby (2014) estimated that for Segue 1 (with a present-day stellar mass of $\sim 500 M_{\odot}$), the galaxy would have hosted ~ 15 core-collapse SNe for a Salpeter IMF compared to $\gtrsim 250$ SNe for the Geha et al. (2013) IMF. Until the behavior of the IMF in the ultra-faint dwarf regime is better understood, the number of SNe expected to have occurred in such systems will be highly uncertain.

5.3. Gas Content

Among the dwarfs discovered since the beginning of SDSS, only Leo T (which we do not consider a UFD; see Section 1.2) contains any neutral gas (Irwin et al. 2007; Ryan-Weber et al. 2008). Stringent upper limits have been placed on the H I content of many of the UFDs using archival data or deep pointed observations with large single-dish telescopes (Grcevich & Putman 2009; Spekkens et al. 2014; Westmeier et al. 2015). For the most nearby dwarfs these limits can be as small as $\sim 100 M_{\odot}$, while for objects at distances of

~ 100 kpc typical limits are $\sim 1000 M_{\odot}$. No ionized gas associated with UFDs has been detected either, but searches for low surface brightness $H\alpha$ emission similar to what has been detected for high-velocity clouds (e.g., Putman et al. 2003; Barger et al. 2012) could be of interest.

The lack of gas in these tiny galaxies is not a surprise, but the mechanism by which they lost their gas is not clear. Plausible hypotheses for gas removal include reionization, supernova feedback, and ram-pressure stripping. Because nearly all currently known UFDs are close to massive galaxies that are likely surrounded by hot gaseous halos, ram-pressure stripping cannot be ruled out. Studies of isolated UFDs, which should be discovered with LSST, may shed light on this issue.

6. THE ULTRA-FAINT END OF THE GALAXY LUMINOSITY FUNCTION

One of the key properties of the population of UFDs, as distinct from the properties of individual objects, is their luminosity function (LF). The relationship between the LF and the mass function of dark matter halos and subhalos encodes the physics of galaxy formation in the smallest halos and places constraints on dark matter models. Moreover, the LF provides the connection between the low luminosity galaxies observed today and their progenitor systems at high redshift, which may play a significant role in reionizing the universe (see Section 9.3).

The observed dwarf galaxy LF is only equal to the true LF if the dwarf galaxy sample is complete over the luminosity range of interest. UFDs, however, vary widely in luminosity, surface brightness, and distance, and many are close to the detection limits of the surveys in which they were discovered. The LF of such systems therefore cannot be computed until the sensitivity of dwarf galaxy searches has been accurately quantified.

Koposov et al. (2008) presented a careful analysis of the detectability of faint dwarf galaxies using an automated search algorithm in the 5th data release (DR5) of SDSS, covering 8000 deg^2 . They found that a significant fraction of the UFDs discovered in SDSS are close to the detection limit of their algorithm. These objects are detected in SDSS data with an efficiency of $\sim 50\%$, indicating that undetected dwarfs are likely to be present in the SDSS footprint. After correcting for incompleteness, Koposov et al. determined that the differential LF of Milky Way satellites can be approximated as $dN/dM_V = 10^{0.1(M_V+5)+1}$ over the absolute magnitude range $-19 < M_V < -2$. Translated into the Schechter form, the corresponding faint-end slope of the LF is $\alpha = -1.25$. The implied total number of satellite galaxies within the virial radius of the Milky Way is 45 at $M_V < -5$ and 85 at $M_V < -2$. For the faintest dwarfs the incompleteness correction is very large, and it depends on the assumed radial distribution of satellites. If faint dwarfs are concentrated close to the Milky Way, then fewer such objects are expected at large distances where they are currently undetectable. Conversely, if the spatial distribution of the lowest luminosity systems is more extended then there may be enormous numbers of similar objects in the outer halo of the Galaxy. While the radial distribution of dwarfs around the Milky Way can be estimated in numerical simulations (e.g., Wang, Frenk & Cooper 2013; Garrison-Kimmel et al. 2017), ultimately it will have to be measured observationally by deeper surveys.

A similar quantification of dwarf galaxy detectability was carried out by Walsh, Willman & Jerjen (2009) on SDSS DR6 imaging, covering 9500 deg^2 . Walsh, Willman & Jerjen used a more sensitive search algorithm that finds all of the SDSS satellites known at the time at $\gtrsim 90\%$ efficiency, but potentially with a correspondingly high false positive rate.

They concluded that the transition between detectability and invisibility as a function of luminosity, surface brightness, and distance is more gradual than calculated by Koposov et al. (2008), and therefore that all of the known dwarfs should have been visible in SDSS even if they were located at significantly larger distances. According to the Walsh, Willman & Jerjen (2009) analysis, searches in the SDSS footprint are complete out to the virial radius of the Milky Way down to $M_V = -6.5$. The extrapolated total number of Milky Way satellites is $\sim 220 - 340$ depending on the adopted detection threshold. Many subsequent studies have used the detection sensitivity derived by Koposov et al. (2008) and/or Walsh, Willman & Jerjen (2009) to estimate the overall size of the Milky Way satellite population, generally predicting that future surveys will discover $\sim 100 - 300$ dwarfs over the entire sky (e.g., Tollerud et al. 2008; Hargis, Willman & Peter 2014; Newton et al. 2018; Jethwa, Erkal & Belokurov 2018).

Unfortunately, no comparable analyses of the detectability of dwarf galaxies have been published since SDSS DR6. Consequently, the sensitivity of the final 5000 deg² of SDSS imaging, the Dark Energy Survey, Pan-STARRS, and other smaller surveys has never been adequately quantified. Given the large number of new satellites discovered since 2009 and their apparently anisotropic distribution on the sky (Drlica-Wagner et al. 2015), updated determinations of the completeness of searches for nearby dwarf galaxies are urgently needed. Until the sensitivity of all significant surveys has been properly quantified, more detailed calculations of the total number of Milky Way satellites, their LF, and their radial and angular distributions cannot be made. What we can say at present is that the observed LF (without an incompleteness correction) peaks at $M_V \sim -4$, suggesting that any real turnover in the LF must be at even fainter magnitudes.

As an illustration of the discovery potential of future imaging surveys, we construct a very simple toy model of satellite detectability. Motivated by the results of Martin, de Jong & Rix (2008) for SDSS and Bechtol et al. (2015) and Drlica-Wagner et al. (2015) for DES, we assume that a satellite must contain at least 20 stars brighter than the detection limit of the survey in order to be identified. We create realizations of satellites with stellar masses corresponding to absolute magnitudes of $M_V = -2, -4, \text{ and } -6$ by randomly selecting the appropriate number of stars from an old, metal-poor mock stellar population. We then determine the median magnitude of the 20th brightest star for each absolute magnitude and calculate out to what distance that star would be detectable for a given survey depth. Note that the depth of a survey for the purpose of searching for stellar overdensities is $\gtrsim 0.5$ mag shallower than the actual 5σ detection limit because colors become uncertain and star-galaxy separation becomes unreliable at fainter magnitudes. Consistent with Koposov et al. (2008) and Walsh, Willman & Jerjen (2009), we find that SDSS should be complete at $M_V \approx -6$ out to beyond the virial radius of the Milky Way. Similarly, DES should be complete down to $M_V \approx -4$ within the virial radius. A complete search of the Milky Way's virial volume to fainter magnitudes will require full-depth LSST images.

7. ORIGIN AND EVOLUTION

7.1. The Formation of Ultra-Faint Dwarfs and the Stellar Mass-Halo Mass Relation

The formation of the first galaxies depends critically on the mechanisms that allow gas to cool to low enough temperatures for star formation to begin (see, e.g., Bromm & Yoshida 2011 and references therein). UFDs may form either in dark matter minihalos of $10^6 -$

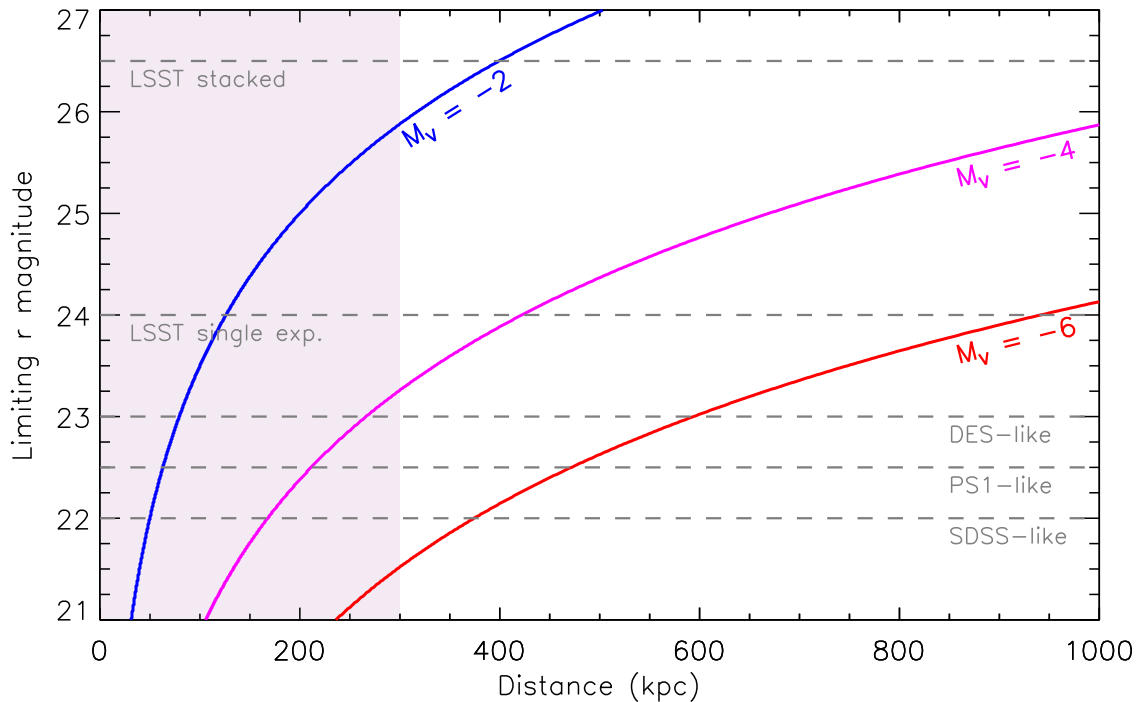


Figure 7 Detectability of faint stellar systems as a function of distance, absolute magnitude, and survey depth. The red curve shows the brightness of the 20th brightest star in an $M_V = -6$ object as a function of distance. The magenta and blue curves show the brightness of the 20th brightest stars for $M_V = -4$ and $M_V = -2$ systems, respectively. The horizontal dashed lines indicate (from bottom to top) the limiting r magnitude for dwarf galaxy searches in SDSS, Pan-STARRS, DES, LSST single exposures, and stacked LSST images at the end of the survey. The region within the (approximate) virial radius of the Milky Way is shaded purple.

$10^8 M_\odot$ (e.g., Bovill & Ricotti 2009; Salvadori & Ferrara 2009), which cool via molecular hydrogen and are thought to be the hosts of the first Population III stars at $z \sim 20$, or in atomic cooling halos of $> 10^8 M_\odot$, which cool initially via atomic hydrogen lines and collapse later at $z \sim 10$ (e.g., Li, De Lucia & Helmi 2010; Frebel & Bromm 2012). Observationally, it may be possible to distinguish these scenarios via either the present-day halo masses of UFDs or their chemical enrichment.

Simulating such tiny galaxies is a difficult computational problem because of the high resolution and high dynamic range needed. There are at least three approaches used in the literature to study small dwarf galaxies theoretically. First, one can directly carry out ultra-high resolution zoom-in simulations of the first galaxies, which explore the physics of the formation and evolution of such systems, but the simulations are generally too expensive to

run to the present day (e.g., Wise et al. 2014; Jeon et al. 2015). Alternatively, simulations of dwarf galaxies located in isolated environments can be run to $z = 0$, at the cost of missing the physics associated with satellite dynamics and stripping (e.g., Simpson et al. 2013; Wheeler et al. 2015). Finally, simulations of satellites of Milky Way-like galaxies may include all of the relevant physics and run to $z = 0$, but are only just beginning to reach the resolution required to study UFDs (e.g., Wetzel et al. 2016; Garrison-Kimmel et al. 2018). In the latter two classes of simulations the properties of the simulated dwarfs are typically in reasonable agreement with observations (e.g., Wetzel et al. 2016; Jeon, Besla & Bromm 2017), but more computing power and higher resolution will be needed to investigate the formation of ultra-faint dwarfs in detail.

One of the most basic questions regarding the formation of dwarf galaxies in a cosmological context is what dark matter halos they occupy. The properties of their dark matter halos control when dwarfs form, their gas content, and their resilience to heating by stellar feedback and reionization. The correspondence between galaxy stellar masses and dark matter halo masses is referred to as the stellar mass-halo mass (SMHM) relation. As emphasized by Buckley & Peter (2017) and Kim, Peter & Hargis (2017), the SMHM relation is the key to understanding most of the so-called small scale challenges to the Λ CDM model (e.g., Bullock & Boylan-Kolchin 2017).

For halo masses below $\sim 10^{12} M_{\odot}$, the SMHM relation is generally described as a power law, $M_{*} \propto M_{\text{halo}}^{\alpha}$ with small scatter (Moster, Naab & White 2013; Behroozi, Wechsler & Conroy 2013). How the relation behaves for stellar masses below $\sim 10^7 M_{\odot}$ (i.e., for classical and ultra-faint dwarfs) is currently a matter of debate. Hydrodynamic simulations suggest very large scatter at these lowest masses, with an increasing fraction of halos remaining completely dark (e.g., Shen et al. 2014; Sawala et al. 2016; Munshi et al. 2017). However, Jethwa, Erkal & Belokurov (2018) argued based on Bayesian fits to the Milky Way satellite LF with a wide variety of SMHM parameterizations that the observational data are matched better without large scatter, and that the fraction of halos hosting observable galaxies must be significant even at quite low masses. Alternatively, Read & Erkal (2018) recently proposed that a relation between the mean star formation rate and halo mass may be better constrained at dwarf galaxy masses than the SMHM relation is. The discovery of additional satellites and completeness analyses of surveys beyond SDSS will offer improved constraints on the matching between halos and UFDs, which may provide the solution to the missing satellite problem (Kim, Peter & Hargis 2017; Read & Erkal 2018).

7.2. Galactic Orbits

The orbits of dwarf galaxies around the Milky Way control both their tidal evolution and potentially their gas loss through ram-pressure stripping or other effects. However, without three-dimensional kinematic information, only weak orbital constraints are possible. By comparing radial velocity measurements with the Via Lactea II N-body simulation, Rocha, Peter & Bullock (2012) were able to determine approximately when the classical and SDSS satellites last crossed the virial radius of the Milky Way, but the specific orbits of each dwarf remained unknown. For the 15 UFD candidates that lack radial velocities (Section 2), even the infall times cannot be measured.

Until very recently, the only published proper motion for a UFD was the ground-based measurement for Segue 1 (the closest dwarf) by Fritz et al. (2018b). However, the situation changed dramatically as soon as the second data release (DR2) from *Gaia* became available.

Gaia Collaboration et al. (2018) measured the proper motion and orbit of Boo I, and Simon (2018), Fritz et al. (2018a), and Kallivayalil et al. (2018) immediately determined the proper motions and orbits of all UFDs for which spectroscopic members were available. At magnitude $G = 16, 17, 18,$ and 19 , *Gaia* DR2 provides typical proper motion uncertainties of $0.09, 0.15, 0.26,$ and 0.51 mas yr^{-1} , respectively (Lindgren et al. 2018), so even a single UFD member star brighter than $G \approx 18$ is sufficient to determine an accurate proper motion for a given galaxy. The corresponding tangential velocity uncertainties are $43, 71, 123,$ and $241(d/100\text{kpc}) \text{ km s}^{-1}$, where d is the distance in kpc. By averaging the proper motions of multiple members, smaller uncertainties can be achieved. Remarkably, the *Gaia* astrometry is so accurate that UFD proper motions can be measured with a combined photometric and astrometric selection even without any spectroscopic membership information (Massari & Helmi 2018; Pace & Li 2018). We are therefore suddenly in the situation where UFD proper motions outnumber radial velocities. For UFDs beyond ~ 150 kpc, the *Gaia* DR2 proper motions are generally consistent with zero, but that can be improved by the identification of additional member stars and by future *Gaia* releases.

Orbits based on full six-dimensional phase space information have now been computed for all of the Milky Way’s ultra-faint satellites with known radial velocities (Gaia Collaboration et al. 2018; Simon 2018; Fritz et al. 2018a; Kallivayalil et al. 2018). The most important orbital parameter is the pericenter distance, which fortunately only depends rather weakly on the assumed gravitational potential of the Milky Way. For the satellites within 100 kpc, the median pericenter is 38 kpc, the pericenter is generally determined to within $10 - 20\%$, and the typical orbital period is several Gyr (Simon 2018; Fritz et al. 2018b). Surprisingly, this orbit modeling reveals that nearly all of the closest dwarfs are currently very close to the pericenters of their orbits. Only Boo I, Willman 1, and Tucana II are more than ~ 5 kpc beyond their pericenter distances (Simon 2018). The most natural explanation for this peculiar positioning is that there is a selection bias against discovering UFDs that are far from their orbital pericenters. If that is the case, then most of the dwarfs found in SDSS, DES, and other surveys must be close to the survey detection limits, as suggested by Koposov et al. (2008), but contrary to the results of Walsh, Willman & Jerjen (2009), Bechtol et al. (2015), and Drlica-Wagner et al. (2015). Deeper surveys should then reveal a significantly larger population of UFDs that are distributed more evenly along their orbits.

The satellites discovered in DES imaging are noticeably concentrated around the Large and Small Magellanic Clouds (Bechtol et al. 2015; Drlica-Wagner et al. 2015). This result led to speculation that many of these objects might have originated as Magellanic satellites and are now being accreted by the Milky Way (Deason et al. 2015; Drlica-Wagner et al. 2015; Jethwa, Erkal & Belokurov 2016; Sales et al. 2017), as originally predicted by D’Onghia & Lake (2008). Based on their space motions and orbits, the most likely dwarfs to have formed in the Magellanic group are Horologium 1, Hyi I, Carina III, and Tucana II (Kallivayalil et al. 2018; Simon 2018).

7.3. Tidal Evolution

Since their discovery, it has frequently been suggested that many UFDs are experiencing significant tidal stripping as they orbit the Milky Way (e.g., Belokurov et al. 2006; Zucker et al. 2006a; Niederste-Ostholt et al. 2009; Muñoz, Geha & Willman 2010; Sand et al. 2012; Kirby et al. 2013a; Roderick et al. 2015; Collins et al. 2017; Simon et al. 2017). The objects upon which this speculation has focused include Hercules, Leo V, UMa I,

UMa II, Segue 1, Segue 2, and Tuc III. The physical reasoning supporting the idea of tidal stripping or tidal disruption for these satellites ranges from morphology (highly elongated shapes; Hercules and UMa I), apparent extratidal features (Hercules, Segue 1, and Tuc III), and possible velocity gradients (Hercules and Leo V) to deviations from the luminosity-metallicity relation (Segue 2).

Now that the orbits of the UFDs are known, the possibility of tidal stripping or tidal disruption can be discussed much more quantitatively. While some stripping of the dark matter from satellite galaxies is inevitable on almost any orbit, they must approach the Milky Way much more closely in order for an appreciable fraction of their stars to be lost (Peñarrubia, Navarro & McConnachie 2008). The tidal radius of a dwarf galaxy is unfortunately not a well-defined quantity, as it varies with time and depends on both the poorly-known mass distribution of the Milky Way and the even more poorly-known mass distribution of the dwarf. In lieu of carrying out detailed numerical experiments for each dwarf, one can approximate the tidal radius as the Jacobi radius (Binney & Tremaine 2008):

$$r_t = \left(\frac{m_{\text{dwarf}}}{3M_{\text{MW}}} \right)^{1/3} d, \quad 3.$$

where m_{dwarf} is the mass of the dwarf galaxy, M_{MW} is the mass of the Milky Way interior to the location of the dwarf, and d is the distance of the dwarf from the Galactic center. However, we also encourage future computational work to model the response of stars within a dwarf to a time-variable external tidal field in a more realistic way.

To conservatively assess stripping, we adopt a heavy ($1.6 \times 10^{12} M_{\odot}$) Milky Way model and assume that the total mass of each dwarf is limited to the measured mass within its half-light radius. Since the actual halo mass of a dwarf is expected to be several orders of magnitude larger in the absence of stripping, this scenario places a lower bound on the tidal radius. Under these assumptions, we calculate that the tidal radius is currently beyond $3R_{1/2}$ for all of the UFDs except Tuc III ($r_t = 2.3R_{1/2}$) and UMa I ($r_t = 2.2R_{1/2}$). The former is not surprising, as Tuc III has an orbital pericenter of only ~ 3 kpc (Erkal et al. 2018; Simon 2018; Fritz et al. 2018b), at which point its tidal radius may be smaller than its present half-light radius. Not coincidentally, Tuc III is also the only UFD that is unambiguously suffering substantial stripping, with clear tidal tails comprising the majority of its stellar mass extending at least 1 kpc from its main body (Drlica-Wagner et al. 2015; Shipp et al. 2018; Li et al. 2018a; Erkal et al. 2018). UMa I, on the other hand, has a pericenter of ≈ 101 kpc (Simon 2018; Fritz et al. 2018b), essentially equal to its current distance. Its tidal radius is therefore at its minimum value now, and the outer $\sim 15 - 20\%$ of its stars may be vulnerable to stripping. Recall, however, that we have made the extreme assumption that the dark matter halo of each dwarf is truncated at its half-light radius. If the halo of UMa I is substantially more extended, as is very likely to be the case, then only minimal stripping of its stars is possible.

For the remaining UFDs with published kinematics, significant stripping generally appears unlikely. At the pericenters of their orbits, Hyi I and Boo I each have $r_t \approx 3R_{1/2}$, which would leave $\approx 10\%$ of their stars unbound. Again, though, more realistic assumptions about the mass and extent of their dark halos would result in no significant stellar stripping. Segue 2 is in danger of stripping if its velocity dispersion is much smaller than the upper limit determined by Kirby et al. (2013a). If $\sigma \lesssim 0.7 \text{ km s}^{-1}$, then its tidal radius would be $\approx 2R_{1/2}$ at pericenter, so tides remain a plausible explanation for its offset from the luminosity-metallicity relation. The more distant dwarfs often regarded as likely to

have been stripped or disrupted, Hercules and Leo V, can only experience tidal stripping if they are on extremely eccentric orbits bringing them within 10 – 20 kpc of the Galactic center. Such an orbit is not currently excluded for Hercules, but is unlikely for Leo V (Fritz et al. 2018b). With larger halo masses these dwarfs would need to pass within a few kpc of the Milky Way to be disrupted. We therefore suggest that alternative explanations for elongated shapes and velocity gradients, such as formation through mergers or puffy disks (e.g., Starkenburg, Helmi & Sales 2016; Wheeler et al. 2017), should be considered before necessarily attributing such properties to Milky Way tides.

8. ULTRA-FAINT DWARFS AS DARK MATTER LABORATORIES

The nature of dark matter is one of the most significant outstanding questions in astrophysics, and the smallest dwarfs may play an outsized role in helping to answer it. In this section we mention some of the ways in which UFDs can constrain dark matter properties and dark matter models. For broader discussions of dwarf galaxies from a dark matter perspective, see, e.g., Porter, Johnson & Graham (2011), Weinberg et al. (2015), Bullock & Boylan-Kolchin (2017), Buckley & Peter (2017), or Strigari (2018).

UFDs can potentially provide insight into dark matter for several reasons:

- They are the most dark matter-dominated systems known. Unlike in larger and more luminous dwarfs (e.g., Brooks & Zolotov 2014; Di Cintio et al. 2014), their baryonic components are likely to have been dynamically negligible at all times. Their inefficient star formation means that feedback should not be powerful enough to alter their internal density structure (e.g., Oñorbe et al. 2015).
- Because of their small sizes, they offer probes of dark matter on smaller scales ($\sim 20 - 30$ pc for the most compact ultra-faint dwarfs) than is possible anywhere else.
- The number of dwarf galaxies orbiting the Milky Way sets a lower bound on the abundance of low-mass dark matter subhalos, which translates to a limit on the allowed mass of warm dark matter particles (e.g., Kennedy et al. 2014).
- With the exception of the Galactic Center and Sagittarius (which they greatly outnumber), they are the closest dark matter halos to us. The combination of their proximity, their high measured densities (e.g., Simon & Geha 2007), and their low astrophysical backgrounds makes them promising targets for indirect detection experiments.
- Their internal dynamics are so gentle that heating by very weak effects is potentially measurable. For example, Brandt (2016) used the presence of a star cluster in Eridanus II to place tight constraints on MACHO dark matter, and Peñarrubia et al. (2016) proposed that wide binary stars may be disrupted by the dark matter potential of a UFD, allowing a measurement of the dark matter density profile.

Because of the arguments listed above, UFDs have attracted a great deal of attention from a broad cross-section of astrophysicists. Their potential to facilitate indirect detection of dark matter has been a particular focus of attention. The majority of indirect detection experiments search for gamma-rays resulting from annihilation of dark matter particles, using either the *Fermi Gamma-Ray Space Telescope* or ground-based atmospheric Cherenkov telescopes. UFDs are prime targets for both types of facilities (e.g., MAGIC Collaboration et al. 2016; Albert et al. 2017; Archambault et al. 2017). The sensitivity of these searches will continue to improve as integration times increase and new observatories such as the

Cherenkov Telescope Array begin operation. Indirect detection searches in UFDs will offer a critical testing ground for possible dark matter signals seen in other parts of the sky (e.g., Abazajian & Keeley 2016). Dark matter annihilation or decay signals could also manifest in dwarf galaxies as synchrotron emission at radio wavelengths (Spekkens et al. 2013; Regis, Richter & Colafrancesco 2017) or as X-ray emission lines (e.g., Jeltema & Profumo 2016).

The holy grail for dark matter research in dwarf galaxies is the conclusive measurement of the inner density profile of a highly dark matter-dominated system. As mentioned above, UFDs are ideal in the sense that they have the highest known dark matter fractions of any galaxies, and their density structure is unlikely to have been affected by stellar feedback. Their disadvantage is that they contain so few stars that there may not be enough dynamical tracers for a robust measurement of the mass distribution. Given the difficulties encountered in analyzing radial velocity data sets containing hundreds to thousands of stars in the classical dSphs, the maximum achievable sample of ~ 100 stars in the most accessible UFDs will not be sufficient to separate a central dark matter cusp from a core. However, the combination of radial velocities and proper motions can provide much more accurate measurements (e.g., Strigari, Bullock & Kaplinghat 2007; Kallivayalil et al. 2015). Measuring proper motions with an accuracy of $\sim 35 \mu\text{as yr}^{-1}$ (5 km s^{-1} at a distance of 30 kpc) for stars as faint as $r \sim 22$ is a daunting task, but may be feasible with extremely large ground-based telescopes or by combining data from space-based facilities such as HST, *Gaia*, JWST, and WFIRST.

9. ULTRA-FAINT DWARFS BEYOND THE MILKY WAY

9.1. Ultra-Faint Dwarfs Around M31

The natural first step in studying UFDs beyond the Milky Way is exploring the vicinity of M31. The Pan-Andromeda Archaeological Survey (PAndAS) has now imaged the M31 halo out to a projected radius of ~ 150 kpc using the Canada-France-Hawaii Telescope (McConnachie et al. 2009), discovering 17 new dwarf galaxies (Martin et al. 2006, 2009, 2016c; Ibata et al. 2007; Irwin et al. 2008; McConnachie et al. 2008; Richardson et al. 2011). An additional 8 dwarfs in the vicinity of Andromeda have also been discovered since 2004, mainly in SDSS and Pan-STARRS (Zucker et al. 2004, 2007; Majewski et al. 2007; Slater, Bell & Martin 2011; Bell, Slater & Martin 2011; Martin et al. 2013b,a). While a handful of these dwarf galaxies may not be true satellites of M31, all of them except Andromeda XXVII (Conn et al. 2012) are likely located within the M31 virial radius. The currently known M31 satellite population reaches as faint as $M_V \approx -6$ (Martin et al. 2016c), including 8 UFDs according to our definition. The sizes and luminosities of the ultra-faint M31 satellites are in excellent agreement with the locus established by Milky Way dwarfs in Fig. 2.

9.2. Surveys Outside the Local Group

Detecting UFDs at even larger distances is difficult because of their low surface brightnesses and small sizes. In the nearest galaxy groups at distances of 3 – 4 Mpc, the most luminous red giants have apparent magnitudes of $r \sim 24.5 - 25$. Since faint dwarfs contain few stars near the tip of the red giant branch, imaging to fainter than 26th magnitude is necessary to identify an ultra-faint dwarf at these distances as an overdensity of resolved stars. In dedicated deep surveys and HST imaging of nearby galaxy clusters, several objects

near or below our magnitude limit separating UFDs from dSphs have recently been discovered, including d0944+69 ($M_V = -6.4$; Chiboucas, Karachentsev & Tully 2009; Chiboucas et al. 2013) in the M81 group, Virgo UFD1 ($M_V = -6.5$; Jang & Lee 2014) in the Virgo cluster, CenA-MM-Dw7 ($M_V = -7.2$; Crnojević et al. 2016a) in the Centaurus A group, MADCASH J074238+652501-dw ($M_V = -7.7$ Carlin et al. 2016) around NGC 2403, and Fornax UFD1 ($M_V = -7.6$; Lee et al. 2017) in the Fornax cluster. Low-surface brightness dwarfs in the Local Volume with luminosities in the UFD regime can also be identified via their diffuse light (e.g., Bennet et al. 2017; Danieli, van Dokkum & Conroy 2018). The sample of UFDs in other environments is still too small and heterogeneous for comparative studies, but the luminosities and radii of these dwarfs seem to be consistent with the properties of the Milky Way satellites shown in Fig. 2.

The first significant sample of UFDs beyond the Local Group will likely be revealed by LSST. The stacked end-of-survey LSST images will reach fainter than 27th magnitude in g and r bands, up to ~ 1 mag beyond the depth of the current state-of-the-art PISCeS (e.g., Sand et al. 2014; Crnojević et al. 2016a) and MADCASH (Carlin et al. 2016) surveys. Extrapolating from current results, LSST should be sensitive to galaxies as faint as $M_V \approx -6$ in galaxy groups at 3–4 Mpc, and even lower luminosity systems in the local field at 1–2 Mpc (e.g., Tollerud et al. 2008; LSST Science Collaboration et al. 2009) via resolved stars. Systematic searches for UFDs throughout this volume will enable the galaxy luminosity function to be probed down to extremely faint absolute magnitudes across a wide range of environments.

In more massive dwarf galaxies ($M_* > 10^7 M_\odot$), population studies demonstrate that star formation is shut off only by environmental effects (Geha et al. 2012). The lack of gas or ongoing star formation among satellites of the Milky Way and M31 suggests that starvation and ram-pressure stripping are the primary mechanisms for environmental quenching down to masses as small as $M_* \approx 10^{5.5} M_\odot$ (Wetzel, Tollerud & Weisz 2015; Fillingham et al. 2015, 2016, 2018). In the ultra-faint regime, however, the available star formation histories show that star formation ended ~ 12 Gyr ago (Brown et al. 2014) even though at least some of the galaxies were likely accreted by the Milky Way more recently (Rocha, Peter & Bullock 2012; Simon 2018; Fritz et al. 2018a). At lower stellar masses, the timing of quenching, N-body-based models, and hydrodynamic simulations all suggest that reionization is responsible for shutting off star formation (Brown et al. 2014; Jeon, Besla & Bromm 2017; Fitts et al. 2017; Rodriguez Wimberly et al. 2019). If this hypothesis is correct, then UFDs can form anywhere and need not be in close proximity to massive galaxies. LSST would therefore be expected to find large numbers of such systems beyond the boundary of the Local Group (Rodriguez Wimberly et al. 2019).

9.3. Connection to Observations of the High-Redshift Universe

In a recent series of important papers, Boylan-Kolchin, Weisz, and collaborators have quantified the correspondence between dwarf galaxies observed today in the Local Group and faint galaxies at high redshift. Boylan-Kolchin et al. (2015) used the observed star formation histories of nearby dwarfs to calculate their ultraviolet (UV) luminosities as a function of time.¹⁰ They showed that reionizing the universe require a significant contribution of

¹⁰At $z = 7$, $M_{UV} = 0.71M_V(z = 0) - 2.71$, such that classical dSphs had UV magnitudes in the reionization era similar to their V-band magnitudes today, while UFDs had high- z UV magnitudes

UV photons from galaxies at least as faint as the Fornax dSph. Even with the *James Webb Space Telescope* such galaxies will not be detectable at $z \sim 7$ (Boylan-Kolchin et al. 2015). Moreover, Boylan-Kolchin et al. (2016) demonstrated via comparison to N-body simulations that the Local Group is comparable in size to the *Hubble* Ultra Deep Field, and is a cosmologically representative volume at dwarf galaxy masses. Weisz & Boylan-Kolchin (2017) then examined the UV LF in the reionization era. Given that the observed properties of UFDs today demonstrate that galaxies as faint as $M_{UV} \sim -3$ existed at high redshift, they showed that if the currently measured faint-end slope of the UV LF ($\alpha \sim -2$; e.g., Livermore, Finkelstein & Lotz 2017) is extrapolated to $M_{UV} = -3$ then UFDs dominate the ionizing photon production of the universe. However, this assumption substantially overpredicts the observed dwarf galaxy population of the Local Group. If the faint-end slope is shallower ($\alpha = -1.25$), as estimated by Kopolov et al. (2008) from SDSS data, then only bright dwarfs contribute to reionization.

This analysis highlights the complementarity between direct observations of the epoch of reionization and studies of the ancient stars in the closest galaxies. Local Group observations can probe the population of typical galaxies orders of magnitude fainter than will be possible at high redshift in the foreseeable future. As described in the preceding sections, these galaxies can also be dissected star by star, with detailed kinematic, chemical, mass, age, and spatial information. On the other hand, the distant universe provides much better statistics, access to a variety of environments, and the opportunity to compare galaxy populations across cosmic time, none of which can be done nearby. At the intersection between the two we can learn about the sources that reionized the universe, the halo masses associated with faint galaxies, and stellar populations and nucleosynthesis in the first galaxies.

10. SUMMARY AND OUTLOOK

Our understanding of the faintest dwarf galaxies has progressed rapidly since their discovery 14 years ago. As described in Sections 1 and 2, even the basic nature of the first ultra-faint dwarfs was unclear for several years. Now, thanks to dedicated follow-up efforts across a wide range of facilities, the velocity dispersions, masses, densities, metallicities, metallicity dispersions, ages, IMFs, proper motions, and orbits of subsets of the known UFDs have been measured. These observations have shown that UFDs are the most dark matter-dominated, oldest, most metal-poor, and most chemically primitive stellar systems known. Concordant theoretical efforts devoted to simulating galaxy formation in low-mass dark matter halos at increasingly high resolution indicate that the faintest dwarfs appear to naturally correspond to the luminous counterparts of the smallest halos capable of sustaining star formation.

Much work remains to be done, of course. No spectroscopy has been obtained for $\sim 1/3$ of the current ultra-faint satellite population, leaving the status of some objects in question, and the highest-quality star formation histories are available for only 6 galaxies. On the theoretical side, simulating the formation and evolution of low-mass dwarfs around a Milky Way-like host to $z = 0$ remains a computational challenge. Analogs to the lowest-luminosity galaxies ($M_* \lesssim 10^3 M_\odot$) have not yet been reliably simulated. Importantly, the census of Milky Way satellites remains significantly incomplete. Even in the most pessimistic predictions, the Milky Way has approximately twice as many dwarf satellites as have been found so far (e.g., Newton et al. 2018). In optimistic scenarios, the total

$\sim 1 - 2$ mag brighter than their present-day optical magnitudes.

population could be nearly an order of magnitude larger. The missing nearby satellites may be revealed in the next few years by ongoing surveys such as MagLiteS (Drlica-Wagner et al. 2016) and the DESI Legacy Imaging Surveys (Dey et al. 2018), but the more distant ones will require deeper imaging (e.g., LSST). Discovering, confirming, and characterizing possibly hundreds of dwarf galaxy candidates will be a very large undertaking for the worldwide community. As an illustration of this challenge, Figure 8 shows color-magnitude diagrams of the very low-luminosity dwarfs Segue 1 ($d = 23$ kpc; $M_V = -1.3$) and Ret II ($d = 32$ kpc; $M_V = -4.0$), along with the approximate spectroscopic limits that can be achieved at medium resolution (for velocities) and high resolution (for chemical abundances) with current facilities. Spectroscopy for comparable systems at much greater distances can only be obtained with 30 m-class telescopes.

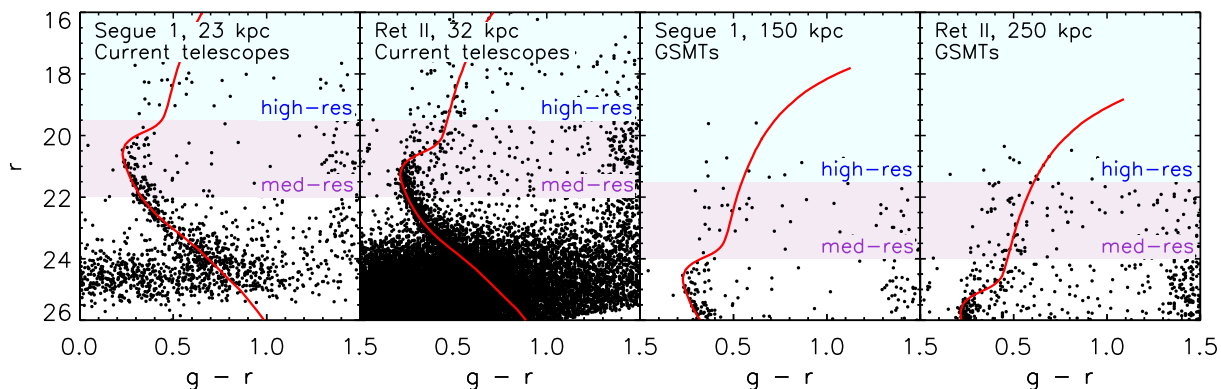


Figure 8 (*left panel*) Color-magnitude diagram of Segue 1 (photometry from Muñoz et al. 2018). The shaded blue and purple magnitude regions indicate the approximate depth that can be reached with existing medium-resolution and high-resolution spectrographs, respectively. (*left middle panel*) Same, but for Ret II (using DES DR1 photometry). (*right middle panel*) Segue 1 shifted to a distance of 150 kpc. With current telescopes only a handful of its stars would be spectroscopically accessible. The shaded blue and purple regions now indicate the depth that could be reached with 30-m telescopes. (*right panel*) Ret II shifted to a distance of 250 kpc, again with the magnitude limits for 30-m telescope spectroscopy.

Looking forward, after completing the census of dwarf galaxies surrounding the Milky Way, stellar kinematics measurements can be used to determine their mass function for comparison with theoretical predictions. Continued chemical reconnaissance via high-resolution spectroscopy may provide new clues to the additional site(s) of r-process nucleosynthesis, and with luck could reveal the signatures of Population III SN explosions. Now that the formation environments of UFDs can be traced by their orbits, precision measurements including an expanded sample of ages from space-based photometry will show how dwarfs that formed in the field or in the Magellanic Group differ from those that have always been close to the Milky Way. Mass and density measurements will provide critical sensitivity and targeting information for indirect detection experiments. Although a detection may seem unlikely given current limits, any signal from dark matter would be of such importance that

the search must continue. Finally, we may hope that astrometry or other novel techniques make it possible to determine the dark matter density profiles of the least-perturbed dark matter halos yet found. This measurement would strongly constrain the properties of dark matter. Given the tremendous amount we have already learned from studying UFDs, it would be fitting if the humblest galaxies in the Universe provided the answer to one of its biggest questions.

FUTURE ISSUES

1. Completing the census of Milky Way satellites. LSST will be needed in order to detect the faintest currently known dwarfs throughout the virial volume of the Milky Way. However, even achieving all-sky coverage (outside the Galactic plane) at SDSS depth or deeper, coupled with well-quantified detection limits, will substantially advance our knowledge of the galaxy luminosity function at faint magnitudes and the likely size of the satellite population of our Galaxy.
2. Obtaining photometric and spectroscopic follow-up observations for as much of the ultra-faint satellite population as possible. These observations are essential for classifying compact, low-luminosity stellar systems and determining their dark matter content. Metallicity and age measurements will enable us to reconstruct their formation and evolution. Expanding the current small sample of galaxies with precise star formation histories is an especially high priority for understanding the effects of reionization and environment on star formation in the faintest dwarfs. Detailed chemical abundance patterns of UFD stars are likely to provide new insight into nucleosynthesis in the early universe.
3. Improving numerical simulations of the smallest galaxies. At present, the computational strategy is often to adjust the physics in simulations in order to reproduce the observed properties of dwarfs. As resolution increases, it should be possible to move beyond this approach and learn about the earliest stages of formation of these systems, and how they evolve in the gravitational potential of the Milky Way. A key result from future simulations will be determining how galaxies populate dark matter halos at masses below $M_{\text{halo}} \sim 10^9 M_{\odot}$.
4. Testing dark matter physics. In addition to placing a lower limit on the mass function of dark matter subhalos, a sample of hundreds of stellar radial velocities and proper motions or other novel ideas could yield tight constraints on the inner density structure of UFD dark matter halos. These measurements would provide a critical test of the cold dark matter prediction that the density profiles of undisturbed dark matter halos should have central cusps.

DISCLOSURE STATEMENT

The author is not aware of any affiliations, memberships, funding, or financial holdings that might be perceived as affecting the objectivity of this review.

ACKNOWLEDGMENTS

We thank Mike Boylan-Kolchin, Marla Geha, Joss Bland-Hawthorn, Alex Ji, Ting Li, and Mike Cooper for helpful suggestions. We are also indebted to Alex Ji for providing his compilation of UFD abundances, which is used in Fig. 6, and to Ting Li for supplying the model stellar population upon which Fig. 7 is based.

This publication is based upon work supported by the National Science Foundation under grants AST-1714873 and AST-1412792. JDS also acknowledges a productive stay during the writing of this article at the Kavli Institute for Theoretical Physics, which is supported in part by the National Science Foundation under Grant No. NSF PHY-1748958, for the program *The Small-Scale Structure of Cold(?) Dark Matter*. This paper would only barely have been possible without NASA's Astrophysics Data System Bibliographic Services.

LITERATURE CITED

- Abazajian KN, Keeley RE. 2016. *Phys. Rev. D* 93:083514
- Adén D, Feltzing S, Koch A, Wilkinson MI, Grebel EK, et al. 2009. *A&A* 506:1147–1168
- Ahnen ML, Ansoldi S, Antonelli LA, Arcaro C, Baack D, et al. 2018. *J. Cosmology Astropart. Phys.* 3:009
- Albert A, Anderson B, Bechtol K, Drlica-Wagner A, Meyer M, et al. 2017. *ApJ* 834:110
- Archambault S, Archer A, Benbow W, Bird R, Bourbeau E, et al. 2017. *Phys. Rev. D* 95:082001
- Audouze J, Tinsley BM. 1976. *ARA&A* 14:43–79
- Barger KA, Haffner LM, Wakker BP, Hill AS, Madsen GJ, Duncan AK. 2012. *ApJ* 761:145
- Battaglia G, Tolstoy E, Helmi A, Irwin M, Parisi P, et al. 2011. *MNRAS* 411:1013–1034
- Battaglia G, Tolstoy E, Helmi A, Irwin MJ, Letarte B, et al. 2006. *A&A* 459:423–440
- Bechtol K, Drlica-Wagner A, Balbinot E, Pieres A, Simon JD, et al. 2015. *ApJ* 807:50
- Behroozi PS, Wechsler RH, Conroy C. 2013. *ApJ* 770:57
- Bell EF, Slater CT, Martin NF. 2011. *ApJ* 742:L15
- Bellazzini M, Ferraro FR, Origlia L, Pancino E, Monaco L, Oliva E. 2002. *AJ* 124:3222–3240
- Bellazzini M, Gennari N, Ferraro FR. 2005. *MNRAS* 360:185–193
- Bellazzini M, Gennari N, Ferraro FR, Sollima A. 2004. *MNRAS* 354:708–712
- Bellazzini M, Ibata RA, Chapman SC, Mackey AD, Monaco L, et al. 2008. *AJ* 136:1147–1170
- Belokurov V, Walker MG, Evans NW, Faria DC, Gilmore G, et al. 2008. *ApJ* 686:L83–L86
- Belokurov V, Walker MG, Evans NW, Gilmore G, Irwin MJ, et al. 2009. *MNRAS* 397:1748–1755
- Belokurov V, Walker MG, Evans NW, Gilmore G, Irwin MJ, et al. 2010. *ApJ* 712:L103–L106
- Belokurov V, Zucker DB, Evans NW, Kleyna JT, Koposov S, et al. 2007. *ApJ* 654:897–906
- Belokurov V, Zucker DB, Evans NW, Wilkinson MI, Irwin MJ, et al. 2006. *ApJ* 647:L111–L114
- Beniamini P, Dvorkin I, Silk J. 2018. *MNRAS* 478:1994–2005
- Beniamini P, Hotokezaka K, Piran T. 2016a. *ApJ* 829:L13
- Beniamini P, Hotokezaka K, Piran T. 2016b. *ApJ* 832:149
- Bennet P, Sand DJ, Crnojević D, Spekkens K, Zaritsky D, Karunakaran A. 2017. *ApJ* 850:109
- Benson AJ, Frenk CS, Lacey CG, Baugh CM, Cole S. 2002. *MNRAS* 333:177–190
- Binney J, Tremaine S. 2008. *Galactic Dynamics: Second Edition*. Princeton University Press
- Bland-Hawthorn J, Karlsson T, Sharma S, Krumholz M, Silk J. 2010. *ApJ* 721:582–596
- Bland-Hawthorn J, Sutherland R, Webster D. 2015. *ApJ* 807:154
- Boettcher E, Willman B, Fadelly R, Strader J, Baker M, et al. 2013. *AJ* 146:94
- Bovill MS, Ricotti M. 2009. *ApJ* 693:1859–1870
- Bovill MS, Ricotti M. 2011. *ApJ* 741:17
- Boylan-Kolchin M, Weisz DR, Bullock JS, Cooper MC. 2016. *MNRAS* 462:L51–L55

- Boylan-Kolchin M, Weisz DR, Johnson BD, Bullock JS, Conroy C, Fitts A. 2015. MNRAS 453:1503–1512
- Bozek B, Fitts A, Boylan-Kolchin M, Garrison-Kimmel S, Abazajian K, et al. 2018. *submitted to MNRAS*
- Brandt TD. 2016. ApJ 824:L31
- Bromm V, Yoshida N. 2011. ARA&A 49:373–407
- Brooks AM, Kuhlen M, Zolotov A, Hooper D. 2013. ApJ 765:22
- Brooks AM, Zolotov A. 2014. ApJ 786:87
- Brown TM, Tumlinson J, Geha M, Kirby EN, VandenBerg DA, et al. 2012. ApJ 753:L21
- Brown TM, Tumlinson J, Geha M, Simon JD, Vargas LC, et al. 2014. ApJ 796:91
- Buckley MR, Peter AHG. 2017. *submitted to Phys. Rep.*
- Bullock JS, Boylan-Kolchin M. 2017. ARA&A 55:343–387
- Bullock JS, Kravtsov AV, Weinberg DH. 2000. ApJ 539:517–521
- Bullock JS, Stewart KR, Kaplinghat M, Tollerud EJ, Wolf J. 2010. ApJ 717:1043–1053
- Calabrese E, Spergel DN. 2016. MNRAS 460:4397–4402
- Caldwell N, Walker MG, Mateo M, Olszewski EW, Koposov S, et al. 2017. ApJ 839:20
- Cannon RD, Hawarden TG, Tritton SB. 1977. MNRAS 180:81P–82P
- Carlin JL, Grillmair CJ, Muñoz RR, Nidever DL, Majewski SR. 2009. ApJ 702:L9–L13
- Carlin JL, Sand DJ. 2018. ApJ, *in press*
- Carlin JL, Sand DJ, Muñoz RR, Spekkens K, Willman B, et al. 2017. AJ 154:267
- Carlin JL, Sand DJ, Price P, Willman B, Karunakaran A, et al. 2016. ApJ 828:L5
- Chabrier G. 2003. PASP 115:763–795
- Chiboucas K, Jacobs BA, Tully RB, Karachentsev ID. 2013. AJ 146:126
- Chiboucas K, Karachentsev ID, Tully RB. 2009. AJ 137:3009–3037
- Chiti A, Frebel A, Ji AP, Jerjen H, Kim D, Norris JE. 2018. ApJ 857:74
- Chornock R, Berger E, Kasen D, Cowperthwaite PS, Nicholl M, et al. 2017. ApJ 848:L19
- Clementini G, Cignoni M, Contreras Ramos R, Federici L, Ripepi V, et al. 2012. ApJ 756:108
- Cohen JG, Christlieb N, Thompson I, McWilliam A, Shectman S, et al. 2013. ApJ 778:56
- Collins MLM, Tollerud EJ, Sand DJ, Bonaca A, Willman B, Strader J. 2017. MNRAS 467:573–585
- Conn AR, Ibata RA, Lewis GF, Parker QA, Zucker DB, et al. 2012. ApJ 758:11
- Conn BC, Jerjen H, Kim D, Schirmer M. 2018. ApJ 852:68
- Cowperthwaite PS, Berger E, Villar VA, Metzger BD, Nicholl M, et al. 2017. ApJ 848:L17
- Crnojević D, Sand DJ, Spekkens K, Caldwell N, Guhathakurta P, et al. 2016a. ApJ 823:19
- Crnojević D, Sand DJ, Zaritsky D, Spekkens K, Willman B, Hargis JR. 2016b. ApJ 824:L14
- Dall’Ora M, Clementini G, Kinemuchi K, Ripepi V, Marconi M, et al. 2006. ApJ 653:L109–L112
- Dall’Ora M, Kinemuchi K, Ripepi V, Rodgers CT, Clementini G, et al. 2012. ApJ 752:42
- Danieli S, van Dokkum P, Conroy C. 2018. ApJ 856:69
- de Jong JTA, Harris J, Coleman MG, Martin NF, Bell EF, et al. 2008. ApJ 680:1112–1119
- Deason AJ, Wetzel AR, Garrison-Kimmel S, Belokurov V. 2015. MNRAS 453:3568–3574
- Dey A, Schlegel DJ, Lang D, Blum R, Burleigh K, et al. 2018. *submitted to AJ*
- Di Cintio A, Brook CB, Macciò AV, Stinson GS, Knebe A, et al. 2014. MNRAS 437:415–423
- D’Onghia E, Lake G. 2008. ApJ 686:L61
- Drlica-Wagner A, Bechtol K, Allam S, Tucker DL, Gruendl RA, et al. 2016. ApJ 833:L5
- Drlica-Wagner A, Bechtol K, Rykoff ES, Luque E, Queiroz A, et al. 2015. ApJ 813:109
- Drout MR, Piro AL, Shappee BJ, Kilpatrick CD, Simon JD, et al. 2017. *Science* 358:1570–1574
- Erkal D, Li TS, Koposov SE, Belokurov V, Balbinot E, et al. 2018. *submitted to MNRAS*
- Errani R, Peñarrubia J, Walker MG. 2018. *submitted to MNRAS*
- Fabrizio M, Merle T, Thévenin F, Nonino M, Bono G, et al. 2012. PASP 124:519
- Feltzing S, Eriksson K, Kleyna J, Wilkinson MI. 2009. A&A 508:L1–L4
- Fillingham SP, Cooper MC, Boylan-Kolchin M, Bullock JS, Garrison-Kimmel S, Wheeler C. 2018. MNRAS 477:4491–4498

- Fillingham SP, Cooper MC, Pace AB, Boylan-Kolchin M, Bullock JS, et al. 2016. *MNRAS* 463:1916–1928
- Fillingham SP, Cooper MC, Wheeler C, Garrison-Kimmel S, Boylan-Kolchin M, Bullock JS. 2015. *MNRAS* 454:2039–2049
- Fitts A, Boylan-Kolchin M, Elbert OD, Bullock JS, Hopkins PF, et al. 2017. *MNRAS* 471:3547–3562
- François P, Monaco L, Bonifacio P, Moni Bidin C, Geisler D, Sbordone L. 2016. *A&A* 588:A7
- Frebel A, Bromm V. 2012. *ApJ* 759:115
- Frebel A, Norris JE. 2015. *ARA&A* 53:631–688
- Frebel A, Norris JE, Gilmore G, Wyse RFG. 2016. *ApJ* 826:110
- Frebel A, Simon JD, Geha M, Willman B. 2010. *ApJ* 708:560–583
- Frebel A, Simon JD, Kirby EN. 2014. *ApJ* 786:74
- Fritz TK, Battaglia G, Pawlowski MS, Kallivayalil N, van der Marel R, et al. 2018a. *A&A*, *in press*
- Fritz TK, Lokken M, Kallivayalil N, Wetzel A, Linden ST, et al. 2018b. *ApJ* 860:164
- Gaia Collaboration, Helmi A, van Leeuwen F, McMillan PJ, Massari D, et al. 2018. *A&A* 616:A12
- Garofalo A, Cusano F, Clementini G, Ripepi V, Dall’Ora M, et al. 2013. *ApJ* 767:62
- Garrison-Kimmel S, Hopkins PF, Wetzel A, Bullock JS, Boylan-Kolchin M, et al. 2018. *submitted to MNRAS*
- Garrison-Kimmel S, Wetzel A, Bullock JS, Hopkins PF, Boylan-Kolchin M, et al. 2017. *MNRAS* 471:1709–1727
- Geha M, Blanton MR, Yan R, Tinker JL. 2012. *ApJ* 757:85
- Geha M, Brown TM, Tumlinson J, Kalirai JS, Simon JD, et al. 2013. *ApJ* 771:29
- Geha M, Willman B, Simon JD, Strigari LE, Kirby EN, et al. 2009. *ApJ* 692:1464–1475
- Gennaro M, Geha M, Tchernyshyov K, Brown TM, Avila RJ, et al. 2018a. *ApJ* 863:38
- Gennaro M, Tchernyshyov K, Brown TM, Geha M, Avila RJ, et al. 2018b. *ApJ* 855:20
- Gilmore G, Norris JE, Monaco L, Yong D, Wyse RFG, Geisler D. 2013. *ApJ* 763:61
- Grcevich J, Putman ME. 2009. *ApJ* 696:385–395
- Greco C, Dall’Ora M, Clementini G, Ripepi V, Di Fabrizio L, et al. 2008. *ApJ* 675:L73
- Grillmair CJ. 2006. *ApJ* 645:L37–L40
- Grillmair CJ. 2009. *ApJ* 693:1118–1127
- Hamanowicz A, Pietrukowicz P, Udalski A, Mróz P, Soszyński I, et al. 2016. *Acta Astron.* 66:197–217
- Hansen TT, Simon JD, Marshall JL, Li TS, Carollo D, et al. 2017. *ApJ* 838:44
- Hargis JR, Willman B, Peter AHG. 2014. *ApJ* 795:L13
- Hargreaves JC, Gilmore G, Annan JD. 1996. *MNRAS* 279:108–120
- Harrington RG, Wilson AG. 1950. *PASP* 62:118–120
- Harris WE. 1996. *AJ* 112:1487
- Hilker M, Richtler T. 2000. *A&A* 362:895–909
- Homma D, Chiba M, Okamoto S, Komiyama Y, Tanaka M, et al. 2016. *ApJ* 832:21
- Homma D, Chiba M, Okamoto S, Komiyama Y, Tanaka M, et al. 2018. *PASJ* 70:S18
- Hopp U, Schulte-Ladbeck RE, Kerp J. 2003. *MNRAS* 339:33–43
- Ibata R, Martin NF, Irwin M, Chapman S, Ferguson AMN, et al. 2007. *ApJ* 671:1591–1623
- Illingworth G. 1976. *ApJ* 204:73–93
- Irwin MJ, Belokurov V, Evans NW, Ryan-Weber EV, de Jong JTA, et al. 2007. *ApJ* 656:L13–L16
- Irwin MJ, Bunclark PS, Bridgeland MT, McMahon RG. 1990. *MNRAS* 244:16P–19P
- Irwin MJ, Ferguson AMN, Huxor AP, Tanvir NR, Ibata RA, Lewis GF. 2008. *ApJ* 676:L17
- Ishigaki MN, Aoki W, Arimoto N, Okamoto S. 2014. *A&A* 562:A146
- Jang IS, Lee MG. 2014. *ApJ* 795:L6
- Jeltema T, Profumo S. 2016. *MNRAS* 458:3592–3596
- Jeon M, Besla G, Bromm V. 2017. *ApJ* 848:85
- Jeon M, Bromm V, Pawlik AH, Milosavljević M. 2015. *MNRAS* 452:1152–1170
- Jethwa P, Erkal D, Belokurov V. 2016. *MNRAS* 461:2212–2233
- Jethwa P, Erkal D, Belokurov V. 2018. *MNRAS* 473:2060–2083

Ji AP, Frebel A, Bromm V. 2015. *MNRAS* 454:659–674
 Ji AP, Frebel A, Chiti A, Simon JD. 2016a. *Nature* 531:610–613
 Ji AP, Frebel A, Simon JD, Chiti A. 2016b. *ApJ* 830:93
 Ji AP, Frebel A, Simon JD, Geha M. 2016c. *ApJ* 817:41
 Ji AP, Simon JD, Frebel A, Venn KA, Hansen TT. 2018. *submitted to ApJ*
 Kallivayalil N, Sales L, Zivick P, Fritz TK, Del Pino A, et al. 2018. *submitted to AAS Journals*
 Kallivayalil N, Wetzel AR, Simon JD, Boylan-Kolchin M, Deason AJ, et al. 2015. *ArXiv e-prints*
 Karczmarek P, Pietrzyński G, Gieren W, Suchomska K, Konorski P, et al. 2015. *AJ* 150:90
 Karlsson T, Bromm V, Bland-Hawthorn J. 2013. *Reviews of Modern Physics* 85:809–848
 Kasliwal MM, Nakar E, Singer LP, Kaplan DL, Cook DO, et al. 2017. *Science* 358:1559–1565
 Kennedy R, Frenk C, Cole S, Benson A. 2014. *MNRAS* 442:2487–2495
 Kim D, Jerjen H. 2015. *ApJ* 808:L39
 Kim D, Jerjen H, Geha M, Chiti A, Milone AP, et al. 2016. *ApJ*, *in press*
 Kim D, Jerjen H, Mackey D, Da Costa GS, Milone AP. 2015a. *ApJ* 804:L44
 Kim D, Jerjen H, Milone AP, Mackey D, Da Costa GS. 2015b. *ApJ* 803:63
 Kim SY, Peter AHG, Hargis JR. 2017. *submitted to Phys. Rev. Lett.*
 Kinemuchi K, Harris HC, Smith HA, Silbermann NA, Snyder LA, et al. 2008. *AJ* 136:1921–1939
 King IR. 1966. *AJ* 71:64
 Kirby EN, Boylan-Kolchin M, Cohen JG, Geha M, Bullock JS, Kaplinghat M. 2013a. *ApJ* 770:16
 Kirby EN, Cohen JG, Guhathakurta P, Cheng L, Bullock JS, Gallazzi A. 2013b. *ApJ* 779:102
 Kirby EN, Cohen JG, Simon JD, Guhathakurta P. 2015. *ApJ* 814:L7
 Kirby EN, Cohen JG, Simon JD, Guhathakurta P, Thygesen AO, Duggan GE. 2017. *ApJ* 838:83
 Kirby EN, Guhathakurta P, Bolte M, Sneden C, Geha MC. 2009. *ApJ* 705:328–346
 Kirby EN, Lanfranchi GA, Simon JD, Cohen JG, Guhathakurta P. 2011. *ApJ* 727:78
 Kirby EN, Martin CL, Finlator K. 2011. *ApJ* 742:L25
 Kirby EN, Simon JD, Cohen JG. 2015. *ApJ* 810:56
 Kirby EN, Simon JD, Geha M, Guhathakurta P, Frebel A. 2008. *ApJ* 685:L43–L46
 Kleyna J, Wilkinson MI, Evans NW, Gilmore G, Frayn C. 2002. *MNRAS* 330:792–806
 Kleyna JT, Geller MJ, Kenyon SJ, Kurtz MJ. 1997. *AJ* 113:624–633
 Kleyna JT, Wilkinson MI, Evans NW, Gilmore G. 2005. *ApJ* 630:L141–L144
 Klypin A, Kravtsov AV, Valenzuela O, Prada F. 1999. *ApJ* 522:82–92
 Koch A, Feltzing S, Adén D, Matteucci F. 2013. *A&A* 554:A5
 Koch A, Hansen T, Feltzing S, Wilkinson MI. 2014. *ApJ* 780:91
 Koch A, McWilliam A, Grebel EK, Zucker DB, Belokurov V. 2008. *ApJ* 688:L13–L16
 Koch A, Wilkinson MI, Kleyna JT, Irwin M, Zucker DB, et al. 2009. *ApJ* 690:453–462
 Komiya Y, Shigeyama T. 2016. *ApJ* 830:76
 Koposov S, Belokurov V, Evans NW, Hewett PC, Irwin MJ, et al. 2008. *ApJ* 686:279–291
 Koposov SE, Belokurov V, Torrealba G, Evans NW. 2015a. *ApJ* 805:130
 Koposov SE, Casey AR, Belokurov V, Lewis JR, Gilmore G, et al. 2015b. *ApJ* 811:62
 Koposov SE, Gilmore G, Walker MG, Belokurov V, Wyn Evans N, et al. 2011. *ApJ* 736:146
 Koposov SE, Walker MG, Belokurov V, Casey AR, Geringer-Sameth A, et al. 2018. *MNRAS* 479:5343–5361
 Kroupa P. 2001. *MNRAS* 322:231–246
 Kuehn C, Kinemuchi K, Ripepi V, Clementini G, Dall’Ora M, et al. 2008. *ApJ* 674:L81
 Laevens BPM, Martin NF, Bernard EJ, Schlafly EF, Sesar B, et al. 2015a. *ApJ* 813:44
 Laevens BPM, Martin NF, Ibata RA, Rix HW, Bernard EJ, et al. 2015b. *ApJ* 802:L18
 Lai DK, Lee YS, Bolte M, Lucatello S, Beers TC, et al. 2011. *ApJ* 738:51
 Lee DM, Johnston KV, Tumlinson J, Sen B, Simon JD. 2013. *ApJ* 774:103
 Lee MG, Jang IS, Beaton R, Seibert M, Bono G, Madore B. 2017. *ApJ* 835:L27
 Lee MG, Park HS, Park JH, Sohn YJ, Oh SJ, et al. 2003. *AJ* 126:2840–2866
 Lee YW, Joo JM, Sohn YJ, Rey SC, Lee HC, Walker AR. 1999. *Nature* 402:55–57

- Li TS, Simon JD, Drlica-Wagner A, Bechtol K, Wang MY, et al. 2017. *ApJ* 838:8
- Li TS, Simon JD, Kuehn K, Pace AB, Erkal D, et al. 2018a. *ApJ*, *in press*
- Li TS, Simon JD, Pace AB, Torrealba G, Kuehn K, et al. 2018b. *ApJ* 857:145
- Li YS, De Lucia G, Helmi A. 2010. *MNRAS* 401:2036–2052
- Lindgren L, Hernández J, Bombrun A, Klioner S, Bastian U, et al. 2018. *A&A* 616:A2
- Livermore RC, Finkelstein SL, Lotz JM. 2017. *ApJ* 835:113
- Longeard N, Martin N, Starkenburg E, Ibata RA, Collins MLM, et al. 2018. *MNRAS* 480:2609–2627
- LSST Science Collaboration, Abell PA, Allison J, Anderson SF, Andrew JR, et al. 2009. *ArXiv e-prints*
- Luque E, Pieres A, Santiago B, Yanny B, Vivas AK, et al. 2017. *MNRAS* 468:97–108
- MAGIC Collaboration, Ahnen ML, Ansoldi S, Antonelli LA, Antoranz P, et al. 2016. *J. Cosmology Astropart. Phys.* 2:039
- Majewski SR, Beaton RL, Patterson RJ, Kalirai JS, Geha MC, et al. 2007. *ApJ* 670:L9–L12
- Majewski SR, Patterson RJ, Dinescu DI, Johnson WY, Ostheimer JC, et al. 2000. *ω Centauri : Nucleus of a milky way dwarf spheroidal ?* In *Liege International Astrophysical Colloquia*, eds. A Noels, P Magain, D Caro, E Jehin, G Parmentier, AA Thoul, vol. 35 of *Liege International Astrophysical Colloquia*
- Majewski SR, Skrutskie MF, Weinberg MD, Ostheimer JC. 2003. *ApJ* 599:1082–1115
- Martin NF, de Jong JTA, Rix HW. 2008. *ApJ* 684:1075–1092
- Martin NF, Geha M, Ibata RA, Collins MLM, Laevens BPM, et al. 2016a. *MNRAS* 458:L59–L63
- Martin NF, Ibata RA, Chapman SC, Irwin M, Lewis GF. 2007. *MNRAS* 380:281–300
- Martin NF, Ibata RA, Collins MLM, Rich RM, Bell EF, et al. 2016b. *ApJ* 818:40
- Martin NF, Ibata RA, Irwin MJ, Chapman S, Lewis GF, et al. 2006. *MNRAS* 371:1983–1991
- Martin NF, Ibata RA, Lewis GF, McConnachie A, Babul A, et al. 2016c. *ApJ* 833:167
- Martin NF, McConnachie AW, Irwin M, Widrow LM, Ferguson AMN, et al. 2009. *ApJ* 705:758–765
- Martin NF, Nidever DL, Besla G, Olsen K, Walker AR, et al. 2015. *ApJ* 804:L5
- Martin NF, Schlafly EF, Slater CT, Bernard EJ, Rix HW, et al. 2013a. *ApJ* 779:L10
- Martin NF, Slater CT, Schlafly EF, Morganson E, Rix HW, et al. 2013b. *ApJ* 772:15
- Martinez GD, Minor QE, Bullock J, Kaplinghat M, Simon JD, Geha M. 2011. *ApJ* 738:55
- Massari D, Helmi A. 2018. *submitted to A&A*
- Mateo M, Olszewski EW, Walker MG. 2008. *ApJ* 675:201–233
- Mateo ML. 1998. *ARA&A* 36:435–506
- McConnachie AW. 2012. *AJ* 144:4
- McConnachie AW, Côté P. 2010. *ApJ* 722:L209–L214
- McConnachie AW, Huxor A, Martin NF, Irwin MJ, Chapman SC, et al. 2008. *ApJ* 688:1009–1020
- McConnachie AW, Irwin MJ, Ibata RA, Dubinski J, Widrow LM, et al. 2009. *Nature* 461:66–69
- Medina GE, Muñoz RR, Vivas AK, Carlin JL, Förster F, et al. 2018. *ApJ* 855:43
- Minor QE, Martinez G, Bullock J, Kaplinghat M, Trainor R. 2010. *ApJ* 721:1142–1157
- Moe M, Kratter KM, Badenes C. 2018. *submitted to ApJ*
- Moore B, Ghigna S, Governato F, Lake G, Quinn T, et al. 1999. *ApJ* 524:L19–L22
- Moretti MI, Dall’Ora M, Ripepi V, Clementini G, Di Fabrizio L, et al. 2009. *ApJ* 699:L125–L129
- Moster BP, Naab T, White SDM. 2013. *MNRAS* 428:3121–3138
- Muñoz RR, Carlin JL, Frinchaboy PM, Nidever DL, Majewski SR, Patterson RJ. 2006. *ApJ* 650:L51–L54
- Muñoz RR, Côté P, Santana FA, Geha M, Simon JD, et al. 2018. *ApJ* 860:66
- Muñoz RR, Frinchaboy PM, Majewski SR, Kuhn JR, Chou MY, et al. 2005. *ApJ* 631:L137–L141
- Muñoz RR, Geha M, Willman B. 2010. *AJ* 140:138–151
- Muñoz RR, Majewski SR, Johnston KV. 2008. *ApJ* 679:346–372
- Mucciarelli A, Bellazzini M, Ibata R, Romano D, Chapman SC, Monaco L. 2017. *A&A* 605:A46
- Munshi F, Brooks AM, Applebaum E, Weisz DR, Governato F, Quinn TR. 2017. *ArXiv e-prints*
- Musella I, Ripepi V, Clementini G, Dall’Ora M, Kinemuchi K, et al. 2009. *ApJ* 695:L83–L87

Musella I, Ripepi V, Marconi M, Clementini G, Dall’Ora M, et al. 2012. *ApJ* 756:121
 Mutlu-Pakdil B, Sand DJ, Carlin JL, Spekkens K, Caldwell N, et al. 2018. *submitted to ApJ*
 Nagasawa DQ, Marshall JL, Li TS, Hansen TT, Simon JD, et al. 2018. *ApJ* 852:99
 Najita J, Willman B, Finkbeiner DP, Foley RJ, Hawley S, et al. 2016. *ArXiv e-prints*
 Newton O, Cautun M, Jenkins A, Frenk CS, Helly JC. 2018. *MNRAS* 479:2853–2870
 Niederste-Ostholt M, Belokurov V, Evans NW, Gilmore G, Wyse RFG, Norris JE. 2009. *MNRAS* 398:1771–1781
 Nomoto K, Kobayashi C, Tominaga N. 2013. *ARA&A* 51:457–509
 Norris JE, Gilmore G, Wyse RFG, Yong D, Frebel A. 2010a. *ApJ* 722:L104–L109
 Norris JE, Wyse RFG, Gilmore G, Yong D, Frebel A, et al. 2010b. *ApJ* 723:1632–1650
 Norris JE, Yong D, Gilmore G, Wyse RFG. 2010c. *ApJ* 711:350–360
 Oñorbe J, Boylan-Kolchin M, Bullock JS, Hopkins PF, Kereš D, et al. 2015. *MNRAS* 454:2092–2106
 Oh KS, Lin DNC, Aarseth SJ. 1995. *ApJ* 442:142–158
 Okamoto S, Arimoto N, Yamada Y, Onodera M. 2008. *A&A* 487:103–108
 Okamoto S, Arimoto N, Yamada Y, Onodera M. 2012. *ApJ* 744:96
 Olszewski EW, Aaronson M, Hill JM. 1995. *AJ* 110:2120
 Olszewski EW, Pryor C, Armandroff TE. 1996. *AJ* 111:750
 Pace AB, Li TS. 2018. *submitted to ApJ*
 Peñarrubia J, Ludlow AD, Chanamé J, Walker MG. 2016. *MNRAS* 461:L72–L76
 Peñarrubia J, Navarro JF, McConnachie AW. 2008. *ApJ* 673:226–240
 Pian E, D’Avanzo P, Benetti S, Branchesi M, Brocato E, et al. 2017. *Nature* 551:67–70
 Piatek S, Pryor C. 1995. *AJ* 109:1071–1085
 Pietrzyński G, Gieren W, Szewczyk O, Walker A, Rizzi L, et al. 2008. *AJ* 135:1993–1997
 Plummer HC. 1911. *MNRAS* 71:460–470
 Porter TA, Johnson RP, Graham PW. 2011. *ARA&A* 49:155–194
 Putman ME, Bland-Hawthorn J, Veilleux S, Gibson BK, Freeman KC, Maloney PR. 2003. *ApJ* 597:948–956
 Read JI, Erkal D. 2018. *submitted to MNRAS*
 Regis M, Richter L, Colafrancesco S. 2017. *J. Cosmology Astropart. Phys.* 7:025
 Richardson JC, Irwin MJ, McConnachie AW, Martin NF, Dotter AL, et al. 2011. *ApJ* 732:76
 Rizzi L, Held EV, Saviane I, Tully RB, Gullieuszik M. 2007. *MNRAS* 380:1255–1260
 Rocha M, Peter AHG, Bullock J. 2012. *MNRAS* 425:231–244
 Roederer TA, Jerjen H, Mackey AD, Da Costa GS. 2015. *ApJ* 804:134
 Rodriguez Wimberly MK, Cooper MC, Fillingham SP, Boylan-Kolchin M, Bullock JS, Garrison-Kimmel S. 2019. *MNRAS* 483:4031–4039
 Roederer IU. 2013. *AJ* 145:26
 Roederer IU, Kirby EN. 2014. *MNRAS* 440:2665–2675
 Roederer IU, Mateo M, Bailey III JI, Song Y, Bell EF, et al. 2016. *AJ* 151:82
 Roederer IU, Preston GW, Thompson IB, Sheckman SA, Sneden C, et al. 2014. *AJ* 147:136
 Romano D, Bellazzini M, Starkenburg E, Leaman R. 2015. *MNRAS* 446:4220–4231
 Ryan-Weber EV, Begum A, Oosterloo T, Pal S, Irwin MJ, et al. 2008. *MNRAS* 384:535–540
 Safarzadeh M, Ji AP, Dooley GA, Frebel A, Scannapieco E, et al. 2018. *MNRAS* 476:5006–5015
 Safarzadeh M, Scannapieco E. 2017. *MNRAS* 471:2088–2096
 Sakamoto T, Hasegawa T. 2006. *ApJ* 653:L29–L32
 Sales LV, Navarro JF, Kallivayalil N, Frenk CS. 2017. *MNRAS* 465:1879–1888
 Salpeter EE. 1955. *ApJ* 121:161
 Salvadori S, Ferrara A. 2009. *MNRAS* 395:L6–L10
 Salvadori S, Skúladóttir Á, Tolstoy E. 2015. *MNRAS* 454:1320–1331
 Sand DJ, Crnojević D, Strader J, Toloba E, Simon JD, et al. 2014. *ApJ* 793:L7
 Sand DJ, Seth A, Olszewski EW, Willman B, Zaritsky D, Kallivayalil N. 2010. *ApJ* 718:530–542
 Sand DJ, Strader J, Willman B, Zaritsky D, McLeod B, et al. 2012. *ApJ* 756:79

- Santana FA, Muñoz RR, Geha M, Côté P, Stetson P, et al. 2013. *ApJ* 774:106
- Sawala T, Frenk CS, Fattahi A, Navarro JF, Theuns T, et al. 2016. *MNRAS* 456:85–97
- Searle L, Sargent WLW. 1972. *ApJ* 173:25
- Shapley H. 1938a. *Harvard College Observatory Bulletin* 908:1–11
- Shapley H. 1938b. *Nature* 142:715–716
- Shappee BJ, Simon JD, Drout MR, Piro AL, Morrell N, et al. 2017. *Science* 358:1574–1578
- Shen S, Madau P, Conroy C, Governato F, Mayer L. 2014. *ApJ* 792:99
- Shipp N, Drlica-Wagner A, Balbinot E, Ferguson P, Erkal D, et al. 2018. *ApJ* 862:114
- Siegel MH, Shetrone MD, Irwin M. 2008. *AJ* 135:2084–2094
- Simon JD. 2018. *ApJ* 863:89
- Simon JD, Blitz L. 2002. *ApJ* 574:726–739
- Simon JD, Drlica-Wagner A, Li TS, Nord B, Geha M, et al. 2015. *ApJ* 808:95
- Simon JD, Frebel A, McWilliam A, Kirby EN, Thompson IB. 2010. *ApJ* 716:446–452
- Simon JD, Geha M. 2007. *ApJ* 670:313–331
- Simon JD, Geha M, Minor QE, Martinez GD, Kirby EN, et al. 2011. *ApJ* 733:46
- Simon JD, Li TS, Drlica-Wagner A, Bechtol K, Marshall JL, et al. 2017. *ApJ* 838:11
- Simpson CM, Bryan GL, Johnston KV, Smith BD, Mac Low MM, et al. 2013. *MNRAS* 432:1989–2011
- Slater CT, Bell EF, Martin NF. 2011. *ApJ* 742:L14
- Smartt SJ, Chen TW, Jerkstrand A, Coughlin M, Kankare E, et al. 2017. *Nature* 551:75–79
- Somerville RS. 2002. *ApJ* 572:L23–L26
- Spekkens K, Mason BS, Aguirre JE, Nhan B. 2013. *ApJ* 773:61
- Spekkens K, Urbancic N, Mason BS, Willman B, Aguirre JE. 2014. *ApJ* 795:L5
- Spencer ME, Mateo M, Walker MG, Olszewski EW, McConnachie AW, et al. 2017. *AJ* 153:254
- Spiniello C, Trager SC, Koopmans LVE, Chen YP. 2012. *ApJ* 753:L32
- Spite M, Spite F, François P, Bonifacio P, Caffau E, Salvadori S. 2018. *A&A*, *in press*
- Starkenburger TK, Helmi A, Sales LV. 2016. *A&A* 595:A56
- Strigari LE. 2018. *Reports on Progress in Physics* 81:056901
- Strigari LE, Bullock JS, Kaplinghat M. 2007. *ApJ* 657:L1–L4
- Strigari LE, Bullock JS, Kaplinghat M, Simon JD, Geha M, et al. 2008. *Nature* 454:1096–1097
- Tinsley BM. 1979. *ApJ* 229:1046–1056
- Tollerud EJ, Bullock JS, Strigari LE, Willman B. 2008. *ApJ* 688:277–289
- Tolstoy E, Hill V, Tosi M. 2009. *ARA&A* 47:371–425
- Tolstoy E, Irwin MJ, Helmi A, Battaglia G, Jablonka P, et al. 2004. *ApJ* 617:L119–L122
- Torrealba G, Belokurov V, Kuposov SE, Bechtol K, Drlica-Wagner A, et al. 2018. *MNRAS* 475:5085–5097
- Torrealba G, Kuposov SE, Belokurov V, Irwin M. 2016a. *MNRAS* 459:2370–2378
- Torrealba G, Kuposov SE, Belokurov V, Irwin M, Collins M, et al. 2016b. *MNRAS* 463:712–722
- Tremonti CA, Heckman TM, Kauffmann G, Brinchmann J, Charlot S, et al. 2004. *ApJ* 613:898–913
- van Dokkum PG, Conroy C. 2010. *Nature* 468:940–942
- Vargas LC, Geha M, Kirby EN, Simon JD. 2013. *ApJ* 767:134
- Venn KA, Irwin M, Shetrone MD, Tout CA, Hill V, Tolstoy E. 2004. *AJ* 128:1177–1195
- Venn KA, Starkenburg E, Malo L, Martin N, Laevens BPM. 2017. *MNRAS* 466:3741–3752
- Vincenzo F, Matteucci F, Vattakunnel S, Lanfranchi GA. 2014. *MNRAS* 441:2815–2830
- Vivas AK, Olsen K, Blum R, Nidever DL, Walker AR, et al. 2016. *AJ* 151:118
- Vogt SS, Mateo M, Olszewski EW, Keane MJ. 1995. *AJ* 109:151–163
- Walker MG, Mateo M, Olszewski EW. 2009. *AJ* 137:3100–3108
- Walker MG, Mateo M, Olszewski EW, Kuposov S, Belokurov V, et al. 2016. *ApJ* 819:53
- Walker MG, Mateo M, Olszewski EW, Peñarrubia J, Evans NW, Gilmore G. 2009a. *ApJ* 704:1274–1287
- Walker MG, Mateo M, Olszewski EW, Sen B, Woodroffe M. 2009b. *AJ* 137:3109–3138

- Walsh SM, Jerjen H, Willman B. 2007. ApJ 662:L83–L86
- Walsh SM, Willman B, Jerjen H. 2009. AJ 137:450–469
- Walsh SM, Willman B, Sand D, Harris J, Seth A, et al. 2008. ApJ 688:245–253
- Wang J, Frenk CS, Cooper AP. 2013. MNRAS 429:1502–1513
- Webster D, Bland-Hawthorn J, Sutherland R. 2015. ApJ 799:L21
- Webster D, Frebel A, Bland-Hawthorn J. 2016. ApJ 818:80
- Webster D, Sutherland R, Bland-Hawthorn J. 2014. ApJ 796:11
- Weinberg DH, Bullock JS, Governato F, Kuzio de Naray R, Peter AHG. 2015. *Proceedings of the National Academy of Science* 112:12249–12255
- Weisz DR, Boylan-Kolchin M. 2017. MNRAS 469:L83–L88
- Weisz DR, Dolphin AE, Skillman ED, Holtzman J, Gilbert KM, et al. 2014. ApJ 789:147
- Westmeier T, Staveley-Smith L, Calabretta M, Jurek R, Koribalski BS, et al. 2015. MNRAS 453:338–344
- Wetzel AR, Hopkins PF, Kim Jh, Faucher-Giguère CA, Kereš D, Quataert E. 2016. ApJ 827:L23
- Wetzel AR, Tollerud EJ, Weisz DR. 2015. ApJ 808:L27
- Wheeler C, Oñorbe J, Bullock JS, Boylan-Kolchin M, Elbert OD, et al. 2015. MNRAS 453:1305–1316
- Wheeler C, Pace AB, Bullock JS, Boylan-Kolchin M, Oñorbe J, et al. 2017. MNRAS 465:2420–2431
- Whiting AB, Hau GKT, Irwin M, Verdugo M. 2007. AJ 133:715–733
- Willman B. 2010. *Advances in Astronomy* 2010:285454
- Willman B, Blanton MR, West AA, Dalcanton JJ, Hogg DW, et al. 2005a. AJ 129:2692–2700
- Willman B, Dalcanton J, Ivezić Ž, Schneider DP, York DG. 2002. AJ 124:2600–2606
- Willman B, Dalcanton JJ, Martínez-Delgado D, West AA, Blanton MR, et al. 2005b. ApJ 626:L85–L88
- Willman B, Geha M, Strader J, Strigari LE, Simon JD, et al. 2011. AJ 142:128
- Willman B, Strader J. 2012. AJ 144:76
- Wilson AG. 1955. PASP 67:27–29
- Wise JH, Demchenko VG, Halicek MT, Norman ML, Turk MJ, et al. 2014. MNRAS 442:2560–2579
- Wolf J, Martínez GD, Bullock JS, Kaplinghat M, Geha M, et al. 2010. MNRAS 406:1220–1237
- Zucker DB, Belokurov V, Evans NW, Kleyna JT, Irwin MJ, et al. 2006a. ApJ 650:L41–L44
- Zucker DB, Belokurov V, Evans NW, Wilkinson MI, Irwin MJ, et al. 2006b. ApJ 643:L103–L106
- Zucker DB, Kniazev AY, Bell EF, Martínez-Delgado D, Grebel EK, et al. 2004. ApJ 612:L121–L124
- Zucker DB, Kniazev AY, Martínez-Delgado D, Bell EF, Rix HW, et al. 2007. ApJ 659:L21–L24